USRP Based Through Wall Radar

By

SANGEETA GOYAL

Under the Supervision of

Dr. SHOBHA SUNDAR RAM

&

Dr. VIVEK ASHOK BOHARA

Indraprastha Institute of Information Technology Delhi

September, 2016

USRP Based Through Wall Radar

By

SANGEETA GOYAL

Under the Supervision of

Dr. SHOBHA SUNDAR RAM

&

Dr. VIVEK ASHOK BOHARA

Indraprastha Institute of Information Technology Delhi

September, 2016

Certificate

This is to certify that the thesis titled "USRP Based Through Wall Radar" being submitted by Sangeeta Goyal to the Indraprastha Institute of Information Technology Delhi, for the award of the Master of Technology, is an original research work carried out by her under my supervision. In my opinion, the thesis has reached the standards fulfilling the requirements of the regulations relating to the degree.

The results contained in this thesis have not been submitted in part or full to any other university or institute for the award of any degree/diploma.

September, 2016

Dr. Shobha Sundar Ram

Dr. Vivek Ashok Bohara

Department of Electronics and Communication

Indraprastha Institute of Information Technology Delhi
New Delhi 110020

Acknowledgment

I am grateful to Dr. Shobha Sundar Ram and Dr. Vivek Ashok Bohara for being an extraordinary advisor who were always there to guide me at difficult stages of research. Their enthusiasm, encouragement and faith in me throughout have been extremely helpful. I sincerely thank them for being my advisor for this period and for helping me positively with their vast knowledge.

I want to thank Mr. Rahul Gupta for his efforts in making me understand the working of USRPs and Labview and Mr. Vibhutesh Kumar Singh for helping me in understanding the concepts of OFDM.

I am thankful to my parents, siblings and friends who have always encouraged me to achieve my goals and supported me in my hard times emotionally and mentally.

I am also grateful to all those people who helped me in collecting data for radar system. Last but not the least; I thank IIIT Delhi for providing an enthusiastic and peaceful atmosphere, well facilitated RF lab to carry on work uninterrupted.

Abstract

Radar systems for detecting the humans present behind the wall are powerful tools for law enforcement, military and elderly care. Walls are complex propagation mediums that introduce attenuation, refraction and multipath to the radar signals. These radar waveforms provide significant attenuation to the signal (from 0 dB to 20 dB one way path loss). Hence, a radar platform that is reconfigurable in terms of carrier frequency, transmitted waveform etc. may be especially useful for test and measurement purposes in a variety of through-wall scenarios. In this work, we have used a software defined radio platform using universal software radio peripheral and Labview to implement a through-wall radar system. We have implemented two waveforms - a continuous wave (CW) signal and an orthogonal frequency division multiplexing (OFDM) signal at a carrier frequency of 3 GHz. A CW radar provides micro-Doppler signatures of humans. An OFDM radar additionally provides range information but due to system constraints, the realized range resolution is poor. Both the radar configurations have been tested in free space and through-wall conditions to detect the presence of one or more humans.

Table of Contents

List of Figures

Chapter 1

1. Introduction

Surveillance and navigation systems like optical and infrared systems are used for tracking of humans [1-2]. These systems work well in line of sight communication but are of limited use in areas where humans are not visible. Radars [3], on the other hand, can operate 24x7 in all weather conditions, have broader coverage and provide high resolution imaging of objects in motion. As a result, they are used in variety of applications such as ground penetrating radars for pipe detection [4-5], weather radar [6], for hostage-rescue operations [7], and for security and law enforcement [8].

Through-wall radar helps in detection, localization, tracking of humans behind the walls [9]. They are used in variety of applications like detecting the velocity profile of human [10], detecting the activity index of elderly by computing a qualitative matric, indicating the amount of movement a person is engaged in a given time interval [11], in homeland security and law enforcement, and in military operations [12].

Radar systems have been implemented on software defined radio platforms such as the Universal Software Radio Peripherals. These platforms are now studied as they provide flexibility in terms of changing radar parameters like carrier frequency, transmitted waveform, sampling rate, modulation and demodulation. Radars were first implemented on USRP in [13]. Since then, different types of radar systems have been implemented using USRP. For example, ground penetrating radar (GPR) was implemented in [14]. [15] Shows the implementation of ice penetrating radar. Quantification of human indoor activity has been carried out in [16,17]. A high resolution radar system for target detection was done in [18].

This thesis implements both continuous wave radar for micro-Doppler extraction and an OFDM radar for providing both range and micro-Doppler information, using the same hardware platform, in free space as well as in through wall scenario. Most of the work in through wall imaging currently focuses on using algorithms such as back-projection [19] and beam forming [20] for detecting objects in the presence of multipath. This thesis uses a single transmitter and a single receiver system. It uses the short time Fourier transform (STFT) to implement the micro-Doppler (m-Dr) signatures of moving

objects. Micro-Doppler signature [21] refers to the Doppler components arising from non-rigid body motion. In addition to the bulk target motion, m-Dr radar image gives information about different parts of the body showing variable motion. These m-Dr signatures are used in detection, tracking and discrimination of targets with motions [22]. Besides humans, it has helped in analyzing and identifying helicopters, tracking small boats in sea, wind turbines as all these moving objects have their unique m-Dr profile.

1.1 Motivation

Through the wall human sensing and localization enables tracking and surveillance of humans for law enforcement purposes. Consider a war situation [23] shown in Figure 1-1, before taking an action it will be helpful to know the exact head count of people, their location, their activity, movement without letting the people behind the wall know that they are being tracked.

Through wall imaging has also proven to be useful in areas affected by fire and/or earthquake [24-25] as shown in Figure 1-2. It helps in speeding up the rescue operation of people buried below the debris or people stuck in fire by locating them.

Figure 1-1: Sensing Through the walls

Walls are dispersive mediums that introduce refraction and multipath to the propagating signal. For an effective detection system, the transmitted frequency has to be kept low to allow better penetration through the walls [26]. Also, as discussed in [12],

signal propagation condition varies depending on the material and type of the wall in application, thus, the choice of an appropriate frequency of operation which provides good penetration and less attenuation becomes vital. But all the above mentioned radar systems are designed to work at a single carrier frequency and waveform with limited flexibility to change these parameters. This thesis deploys a through-wall radar system using universal software radio peripheral (USRP) that allows the flexibility of changing the above mentioned parameters.

Figure 1-2: Through wall radar applications in different scenarios

1.2 Problem Statement and objectives

Micro-Doppler extraction is been carried using continuous wave (CW) and Orthogonal frequency division multiplexing (OFDM) signals in free space and in through wall. Both free space and through wall require the same processing. CW radar provides velocity profile while OFDM gives range and velocity information as well as micro-Doppler signatures

The main objectives of this thesis can be summarized as:

1. Implementation of CW radar for micro-Doppler extraction in free space and in through-the-wall scenario.
2. Implementation of OFDM radar for extracting the range-Doppler information in free space and in through-the-wall scenario
3. Micro-Doppler extraction using OFDM radar in free space and in through-the-wall scenario

1.3 Thesis Outline

Chapter 2 of this thesis discusses the usefulness of USRP as a platform for a radar system and also talks about the other hardware components used in this thesis. Chapter 3 discusses the methodology, challenges faced and solutions. Experimental setup and implementation results are shown in chapter 4. Chapter 5 concludes the thesis with future work being discussed in chapter 6.

Chapter 2

2. Universal Software Radio Peripheral

The radar system here is implemented on a universal software radio peripheral (USRP). USRP is a software defined radio (SDR), which implements the physical layer functions into software rather than hardware. It is connected to a host computer via. Ethernet cable or a PCIe cable. The platform provides a powerful wireless prototyping system [27]. Although originally designed for the implementation of communication systems, USRP is now used for implementing radar systems as the radio front ends of communication system and radar system are the same.

This thesis uses USRP 2953R for the implementation of radar system along with Labview, a software offered by National Instruments. USRP Rio is a reconfigurable I/O (RIO) architecture, delivering an integrated hardware and software solution, prototyping high performance wireless systems. USRP Rio contains an X300 daughterboard which provides a maximum bandwidth of 40 MHz. Figure 2-1 [28] shows the block diagram of the USRP. It has a state-of-the-art 2x2 MIMO RF transceiver with a LabVIEW programmable DSP oriented Kintex 7 FPGA [28]. It has 2 full duplex channels.

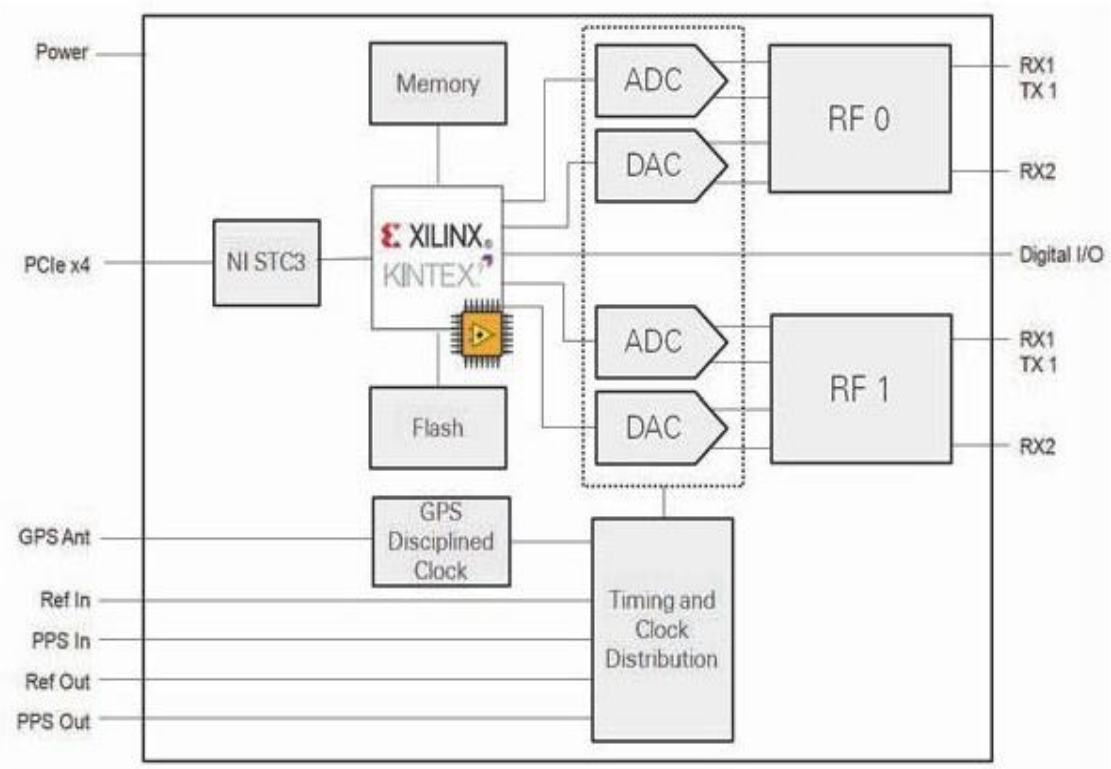

Figure 2-1: Block Diagram of USRP Rio 2953R

Each RF channel includes a switch allowing for time division duplex (TDD) operation on a single antenna using the TX1/RX1 port, or frequency division duplex (FDD) operation using two ports, TX1 and RX2 [29]. Rio works as a transceiver which provides a tunable center frequency from 1.2 GHz to 6 GHz. The maximum output power provided by the device is 17 dBm to 20 dBm for a frequency range of 1.2 GHz to 3.5 GHz and 7 dBm to 15 dBm for a frequency range of 3.5 GHz to 6 GHz. Maximum sampling rate provided by USRP is 120 MS/s and a 16 bit DAC. Maximum input power is -15 dB with 14 bit ADC present at the receiver. Figure 2-2 [28] shows the typical streaming application of USRP Rio driver.

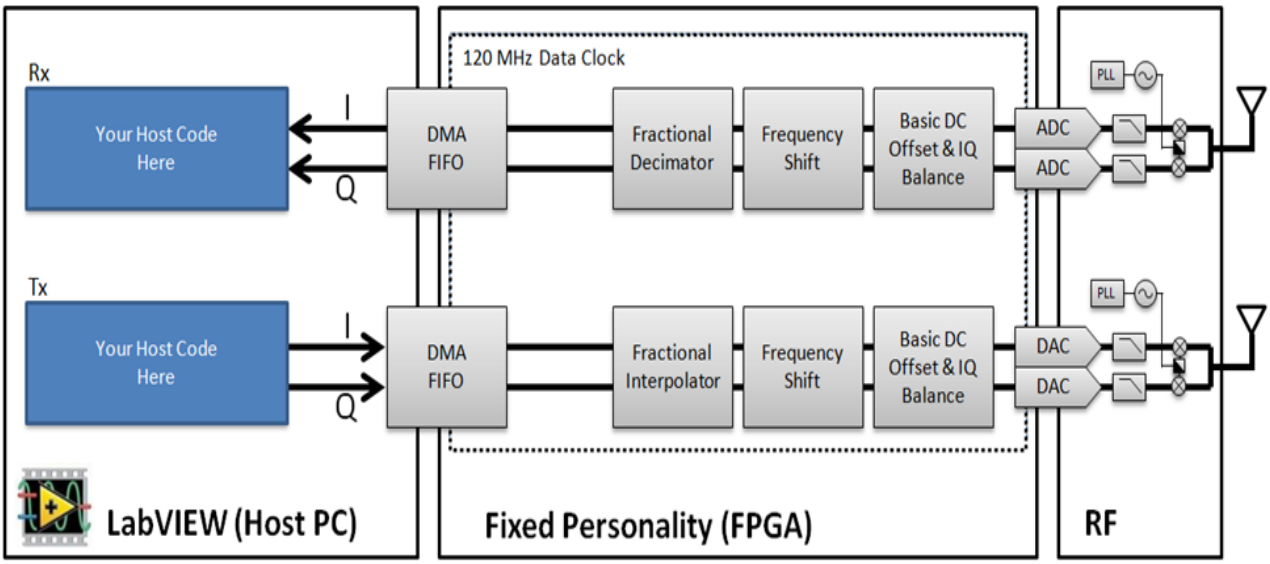

Figure 2-2: Typical Streaming Application Using NI-USRP Driver (Host Only)

The antennas used for the implementation of this thesis are HF907 Double-Ridged horn antennas [30]. These are broadband antennas, working at a frequency range of 0.8 GHz to 18 GHz, and have linear polarization providing frequency dependent gain from 5 dBi to 14 dBi.

Chapter 3

3. Working Methodology

3.1 Initial Experiments

NI offers several USRP platforms, some of which are unsuitable for realizing the radar architectures. For instance, the NI USRP 2921 is half duplex [31]. It has an RF switch that will allow either transmit or the receive operation to occur at any time instant on a same shared antenna as shown in **Error! Reference source not found.** [31]. But since we are implementing a CW radar, that requires both transmit and the receive operation to be performed simultaneously, this platform is therefore unsuitable for the implementation of continuous wave radar.

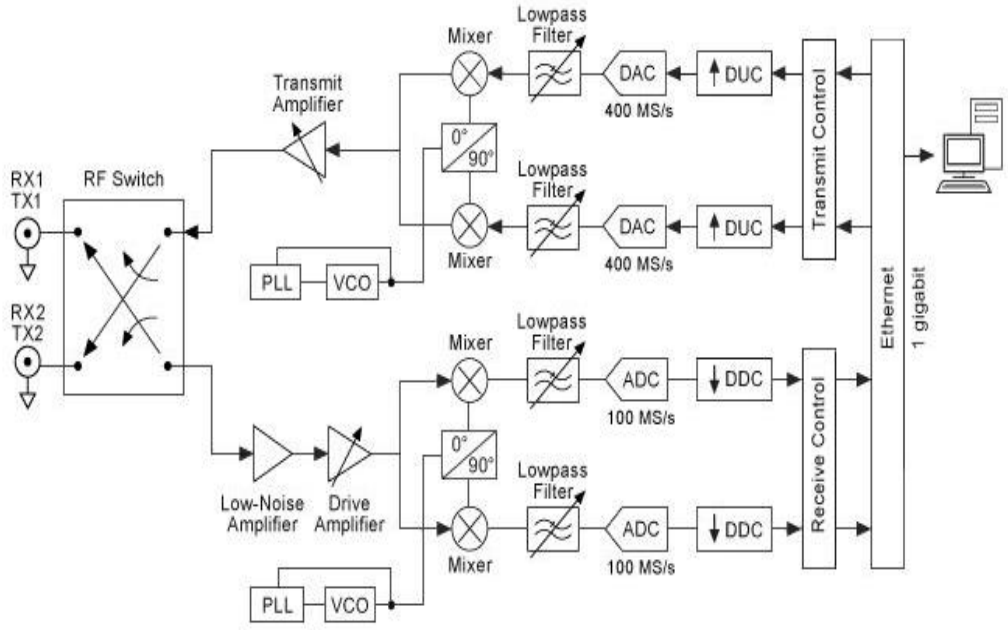

Figure 3-1: Block diagram of USRP 2921

The NI USRP 2922, on the other hand, is full duplex. Figure 3-2 shows the block diagram of USRP 2922 [32]. The RF switch allows transmit and receive operation to be carried out on a single antenna. This can be achieved by using TX1/RX1 port. In 2922, an additional RX2 port is designated in receiver mode only which was not present in USRP 2921. With RX2 port, in USRP 2922, we have separate transmit and receive chains and hence it allows simultaneous transmission and reception, thus allowing the implementation of CW radar.

However, there are two separate oscillators in the two ports. As a result, when this USRP is operated as radar, a frequency offset between the transmitter and receiver oscillators may introduce an error in the operation. Figure 3-3 (a) shows the setup that we used for testing for this offset. Here TX1 port was connected to the RX2 port using an

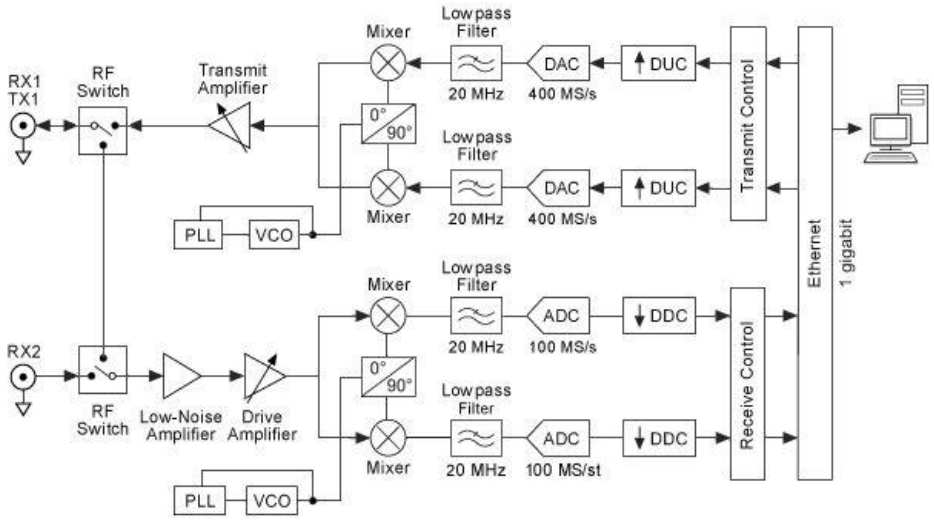

Figure 3-2: Block diagram of USRP 2922

SMA cable and a 30 dB attenuator to protect the receiver circuitry. A signal of frequency 20 KHz was transmitted. It is seen from Figure 3-3 (b) that no frequency offset was present in transmitter and receiver chain of 2922.

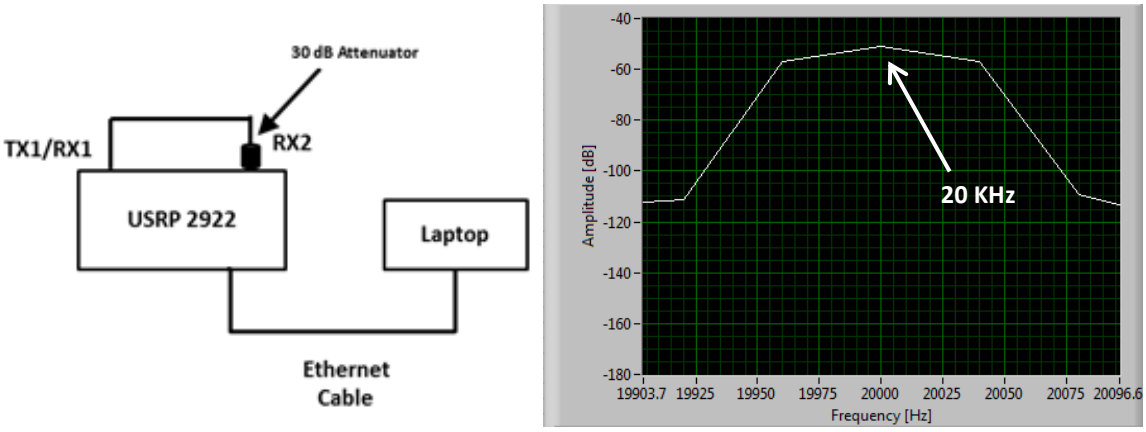

Figure 3-3: (a) Setup, (b) No frequency offset was found between TX and RX chain

Therefore, we implemented the CW Doppler radar on this platform. Both the wired (with 30 dB attenuator) and wireless configurations (without 30 dB attenuator) are showing same power levels as can be seen from Figure 3-3 (b) and Figure 3-4. We inferred that high cross-talk is present between the transmitter and the receiver chains as

both are isolated by a 20 dB pad. Hence the receiver got saturated by the transmitter and this platform also proved to be unsuitable for implementation of radar system.

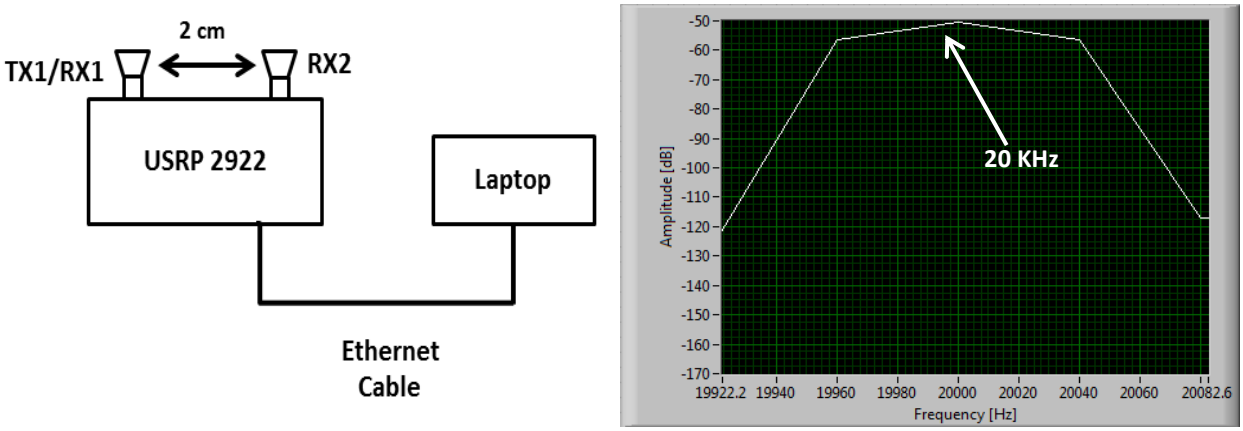

Figure 3-4: Received waveform in presence of moving object

To overcome this limitation, we implemented the radar system using two USRP 2922. However, the transmitter and receivers oscillators are not synchronized and have a different frequency offset each time the systems are started. This was tested by sending an IF signal of 40 KHz and the signal received is at 48880 KHz as shown in Figure 3-5. Both the USRPs may be synchronized using external reference signals with additional hardware complexity. This option was not explored.

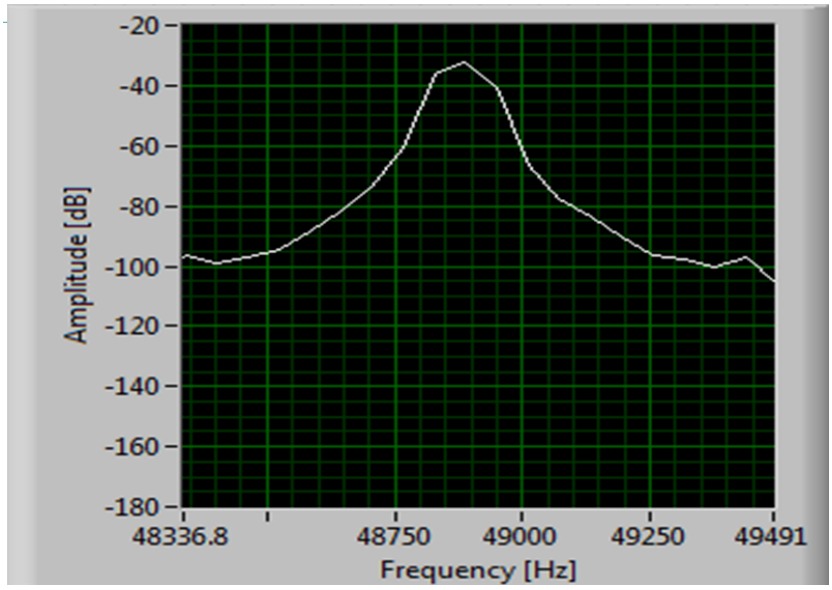

Figure 3-5: Frequency offset between two USRPs

The USRP RIO-2953, provides good isolation between the transmitter and receiver sections and proved to be suitable for radar implementation. We have used two USRPs, one for transmitting and another for receiving. Since the USRP does not provide

any mechanism to measure received and/or transmitted power, the maximum transmitted power was measured using a CXA signal analyzer N9000A. The minimum detected power was measured using N5181A MXG analog signal generator (100 KHz – 3 GHz). Figure 3-6 shows the block diagram of the hardware set up used for measurements.

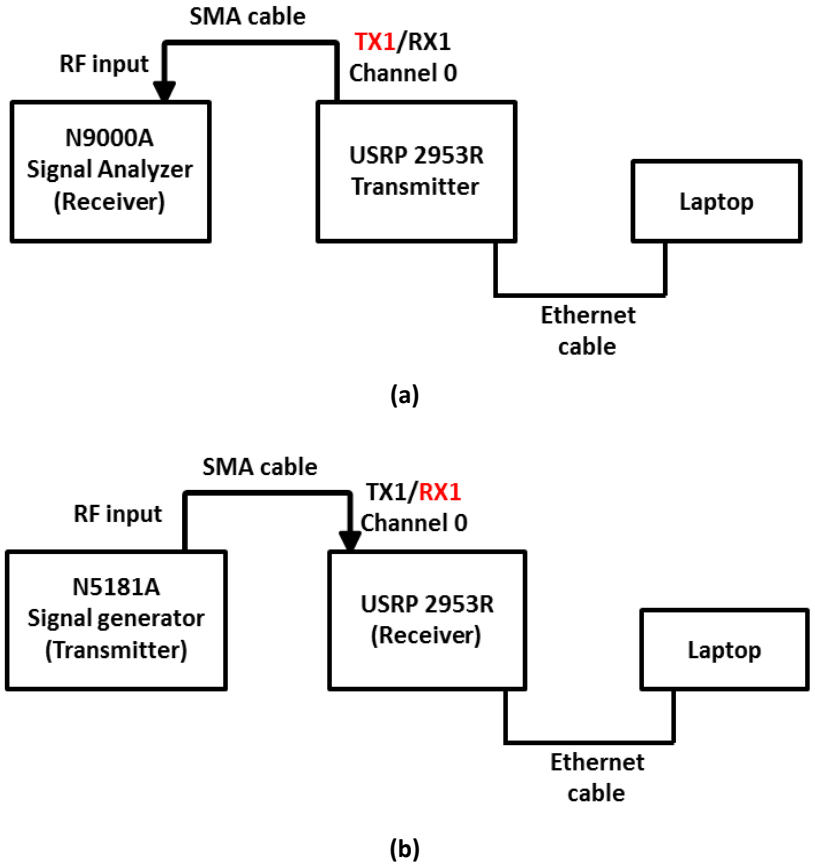

Figure 3-6: (a) Block diagram to measure maximum transmitted power. (b) Block diagram to measure minimum detectable received power

The peak transmitted power is observed to be 17 dBm at frequency of 3 GHz, while minimum received power is -70 dBm (without taking receiver LNA gain into consideration), after that the receiver ADC got saturated. If the antenna gain is assumed to be 8 dBi, then maximum detectable range is of 80 m. A link budget analysis has been done to count for the losses due to the cables and the connectors used. Using the radar range equation, losses can be accounted using eq. (3.1)

$$L = \frac{P_{Tx} G_{Tx} G_{Rx} \lambda^2 \sigma}{(4\pi)^3 R^4 P_{Rx}} \tag{3.1}$$

Where,

P_{tx}= 7 dBm @3 GHz

P_{rx}= -95 dBm

$G_{tx} = G_{rx} = 8$ dBi

$\lambda = 0.1\ m$

$\sigma = 1\ m^2$

$R = 25\ m$

This results in a total loss of 9.1061 dB. This is the loss due to 2 N (M)-N (M) cable, 2 SMA (M)-SMA (M) cable, 2 SMA F-F connector, 2 SMA M-M connector, 2 N (F)-SMA (M) connector.

The system was tested for radar return signals up to 25 m in free space. Also, the peak transmitted power is frequency dependent; hence, it was measured using the same setup shown in Figure 3-6 (a). Figure 3-7 shows the maximum transmitted power at different frequencies.

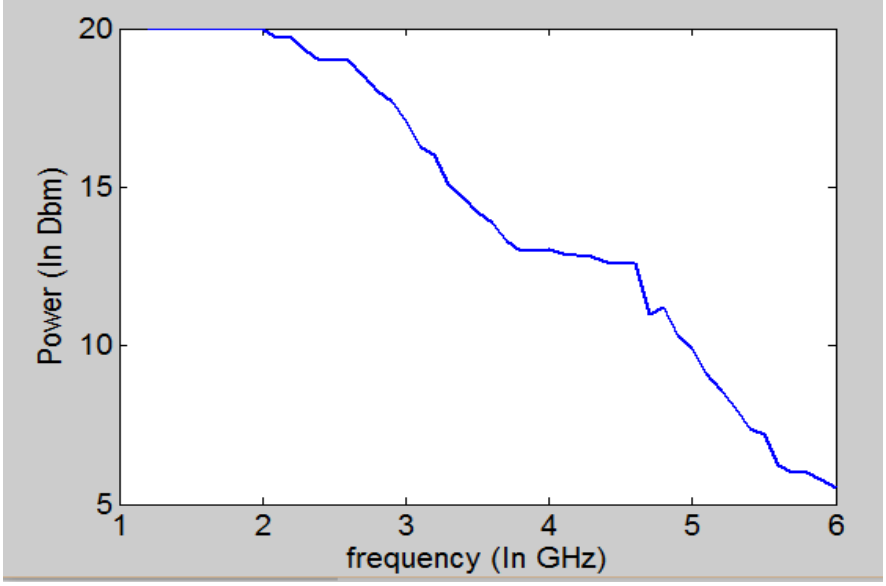

Figure 3-7: Maximum transmitted power at different frequency

Also as the signal propagation depends on the wall conditions as well as the signal, the attenuation provided by a brick wall of 12 inches was measured. The setup used for the measurement is shown in Figure 3-8. First the received power was calculated when there is no wall present between the transmitter and the receiver and then the received power was calculated when wall is present between the transmitter and the receiver.

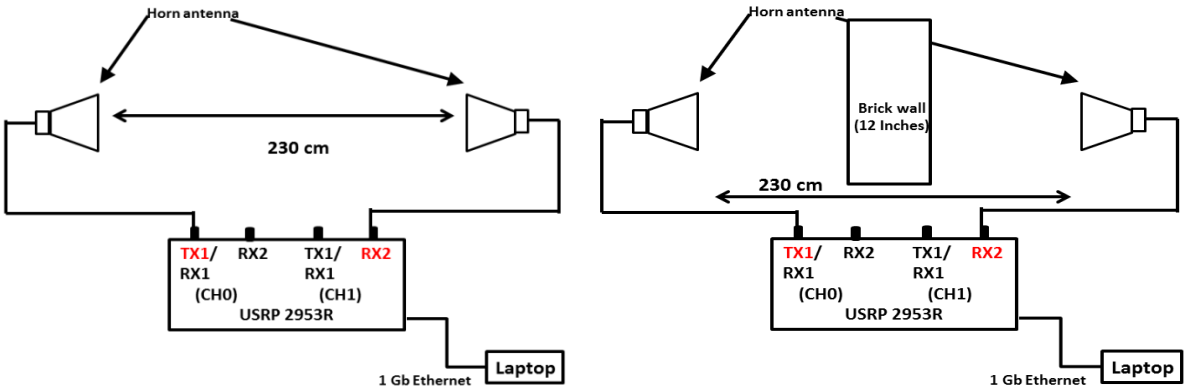

Figure 3-8: Setup used to calculate the attenuation due to the wall

Attenuation due to the wall was then calculated as shown in Figure 3-9. It was seen that a 12 inches brick wall provides an attenuation of 14 dB at 3 GHz.

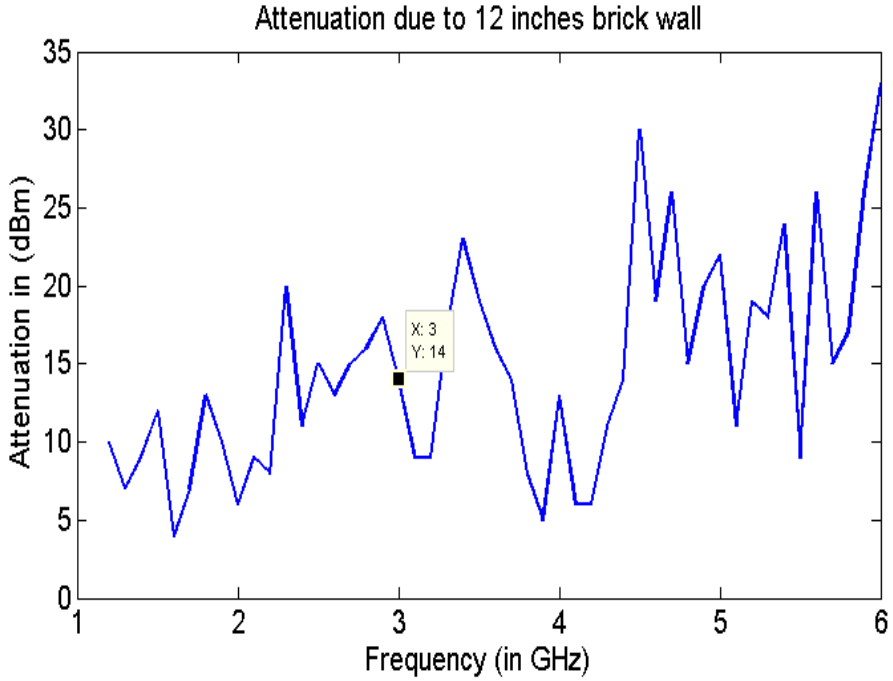

Figure 3-9: Attenuation due to 12 inches brick wall

When we implemented the homodyne CW architecture, we observed a large noise component at frequencies below 10 KHz as shown in Figure 3-10. This can mostly be attributed to flicker noise which results in reduced sensitivity at small Doppler [33]. An improvement of direct CW radar is the super heterodyne radar in which two stage mixers are used.

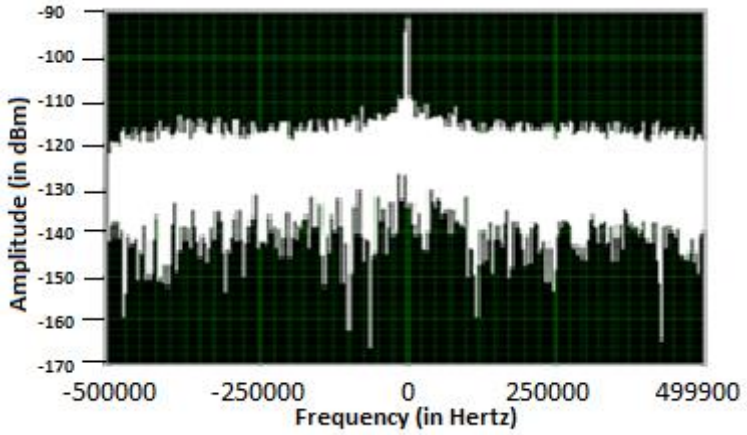

Figure 3-10: Behavior of USRP for homodyne CW architecture

3.2 Super Heterodyne Radar

Figure 3-11 below shows the block diagram of the super heterodyne radar. The RF echo signals are first converted to an intermediate frequency (IF) which is well above the flicker noise. This flicker noise of the first mixer stage cannot pass through the bandpass filter of the IF amplifier. Only in the second mixer, the echo signal is converted into the baseband. Since the amplified echo signal is now much larger than the flicker noise of the second mixing stage, the impact of the noise of the second mixer is reduced.

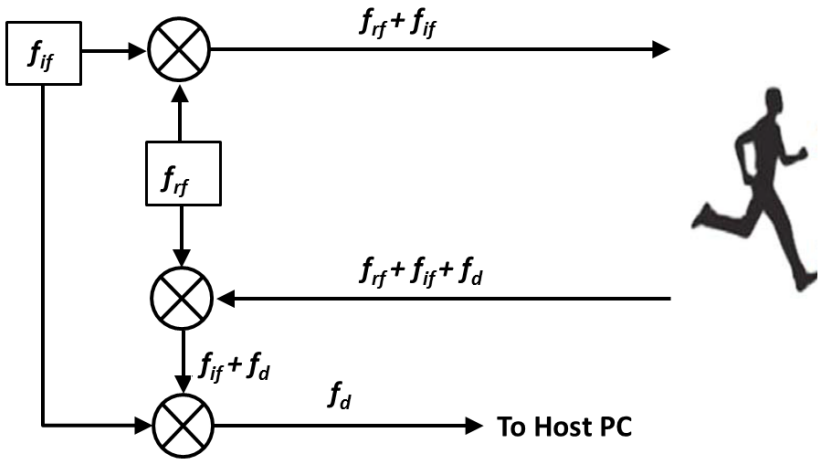

Figure 3-11: Super heterodyne Doppler radar

3.3 Doppler Radar

Doppler radars are narrow band radars which are used to estimate the target's velocity. The frequency of the signal backscatter from a moving object is shifted. This change in frequency is proportional to the velocity of the moving object. If the target is moving with a velocity of v *m/s* then, the Doppler shift observed is given in eq. (3.2)

$$f_d = \frac{2vf_c}{c} \tag{3.2}$$

Where,

f_d is the Doppler shift

f_c is the transmitted signal frequency

c is the speed of light (3e8 m/s) and

v is the radial velocity of the object.

The maximum f_d that can be detected in case of CW radar is given by half of the sampling rate and the frequency resolution is equal to the reciprocal of the sweep time, where sweep time is defined as the total time for which the target has been observed. Depending on the direction of the target, i.e. whether the target is approaching the radar system or moving away from the radar system, the signal frequency increases or decreases respectively.

While implementing CW radar, the direct leakage from transmitter to the receiver is to be avoided and the transmitter and receiver must be synchronized. Direct signal between transmitter and receiver can be removed either by separating the transmitting and receiving antennas or the separation can be done in frequency domain. Here we have two separate transmitter and receiver and the time domain signal is collected for further processing.

For human detection, the received signal is the combined reflections from all the body components in motion, including arms, legs, torso, etc., all of which will be moving at different speeds as shown in eq. (3.3)

$$y(t) = \sum_n a_n e^{i2\pi f_{dn} t} \tag{3.3}$$

Where a_n refers to the amplitude of the received signal and f_{dn} is the received frequency due to different body components. This swinging motion of the hands, legs of the main bulk body motion is known as micro-Doppler [21]. For getting the micro-Doppler information, short time frequency transform (STFT) [36] is applied on the collected received signal given by eq. (3.4)

$$x(\tau, f) = \int y(t) h(\tau - t) e^{-j2\pi f t} dt \tag{3.4}$$

Here, *h(t)* is the window function. STFT, $x(\tau, f)$, provides information in both the time and frequency domains and thus helps in extracting the micro-Doppler signatures of the human.

In this thesis, an intermediate frequency, f_{if} of 40 KHz is used. This signal is mixed with a carrier frequency of 3 GHz. A sampling rate of 400 Kilo samples per second (KS/s) is chosen as this is the minimum frequency provided by USRP. At the receiver of the USRP, the 3 GHz signal is removed at the mixer of the USRP. Intermediate frequency is then removed afterwards in MATLAB using I/Q demodulation done in software. Due to the high sampling frequency, a decimation factor of 400 was chosen. A decimation of 400 will down sample the signal from 400 KHz to 1000 Hz and the maximum Doppler that can be seen using this sampling frequency is -500 Hz to 500 Hz. Human have a maximum Doppler of around 300 Hz and thus down sampling helps in saving computational time. To get the time-varying Doppler information of human motion, STFT is carried out with a window size of 0.1 – 0.12 seconds. This window size is chosen as humans are slow moving targets who have almost constant velocity over a time period of 0.1 seconds. Figure 3-12 shows the implementation of super heterodyne radar for the extraction of micro-Doppler signatures using USRP.

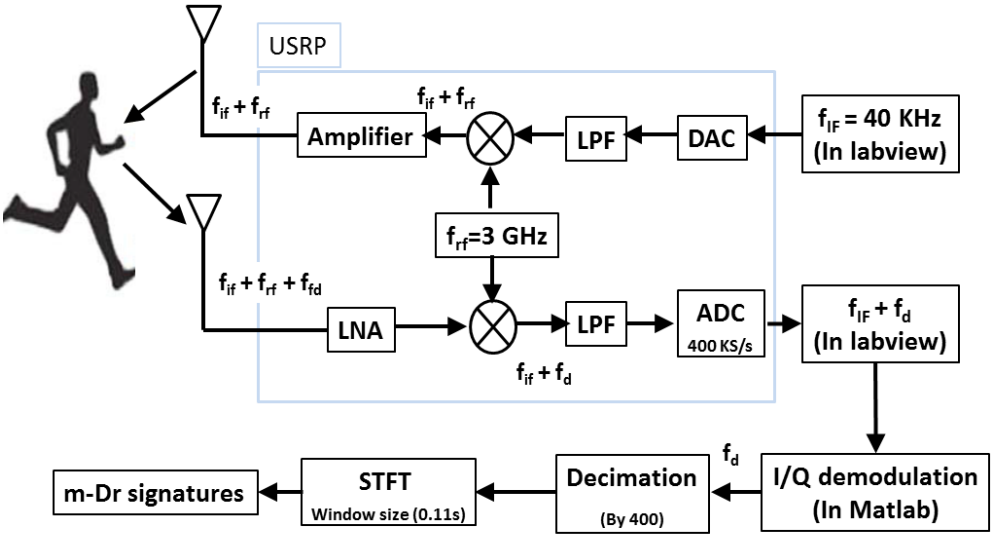

Figure 3-12: Block diagram to implement super heterodyne radar for extracting m-Dr signatures

3.4. OFDM Radar

CW radars are narrow band radars that provide only Doppler information but no range information i.e. the distance between the target and the radar. Wide band radars using waveforms such as chirp and OFDM are able to provide both range and Doppler information. OFDM provides advantage over chirp signal as it uses multiple orthogonal sub-carriers and hence allows for independent and unambiguous range-Doppler processing [37]. OFDM radar using correlation, implemented in [38], requires high

computation efforts. Element wise division technique, used in [39], eliminates the correlation based signal processing and provides lower side lobe levels. This algorithm, irrespective of actual transmitted data, works on complex modulated symbols.

In OFDM, a wideband signal is divided into parallel orthogonal narrowband subcarriers. The time domain expression for the baseband representation OFDM is given by

$$x(k)=\sum_{m=0}^{M-1}\sum_{n=0}^{N-1} D_{Tx}(mN+n)e^{\left(\frac{i2\pi nk}{N}\right)}, \quad \text{where } 0 \le k \le N-1 \tag{3.5}$$

Here, $\frac{k}{N} = f_n t$, and f_n defines the subcarrier bandwidth of the signal.

Where *N* represents the total number of orthogonal subcarriers, *M* the total number of evaluated symbols, $D_{Tx}(mN+n)$ are the symbols modulated with discrete phase modulation technique. For maintaining the orthogonality of the OFDM symbols, and thereby reducing the interference between the subcarriers, the condition given in eq. (3.6) has to be maintained.

$$f_n = n\Delta f = \frac{n}{T}, where, \Delta f = \frac{BW}{N} = \frac{1}{T} \tag{3.6}$$

BW here represents the bandwidth of the OFDM symbol and T is the OFDM symbol duration. Due to the presence of a pulse shaping filter, the spectrum of each sub carrier has a shape of *sin(x)/x*. Thus the entire OFDM symbol spectrum consists of a total of *N sin(x)/x* functions and is given by eq. (3.7)

$$x(f) = \sqrt{t}\sum_{n=0}^{N-1} D_{tx}(n)\frac{\sin(\pi(f-f_n)T)}{(\pi(f-f_n)T)} \tag{3.7}$$

The Figure 3-13 shows the implementation of OFDM transmitter, implemented by mapping bits into modulation symbols, series to parallel converter and IFFT block.

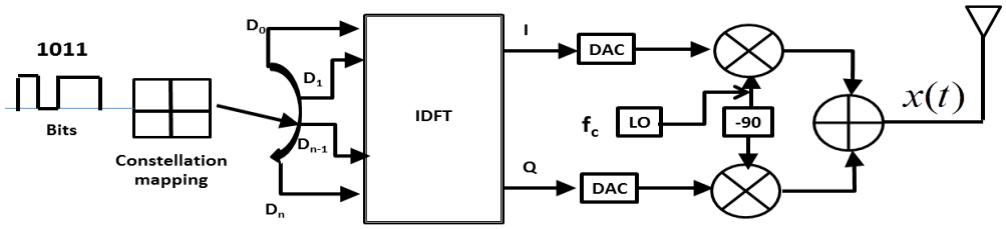

Figure 3-13: OFDM Transmitter

For implementing OFDM receiver, steps are inverted, i.e. first signal is digitized then converted from series to parallel and then DFT is taken over symbols. Figure 3-14 shows the typical OFDM receiver.

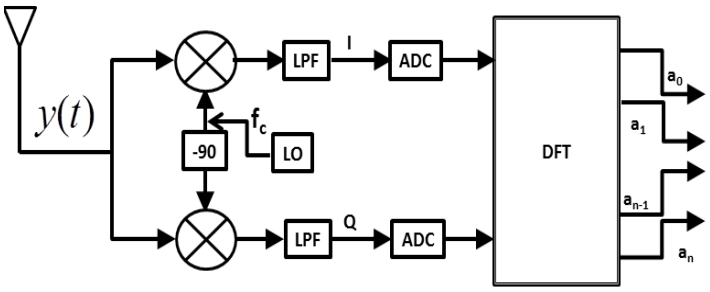

Figure 3-14: OFDM Receiver

Radar processing using OFDM uses modulation symbols, thus reducing the complexity. Range-Doppler processing is independent and one does not relate to the other [40]. Hence both can be done simultaneously. The main disadvantages of OFDM are their sensitivity to inter-symbol interference (ISI) and inter-carrier interference (ICI). One of the main reasons for ICI is loss of synchronization caused by frequency offset between oscillators at the transmitter and the receiver. This causes the carriers to lose orthogonality, so they cannot be separated completely at the receiver. As a consequence, ICI lowers the signal-to-noise ratio (SNR) and increases the error probability. ICI affects the performance when used in communication systems as the transmitter and receiver are located far apart, while in radars, we have synchronized transmitter and receiver as shown in Figure 3-15 and hence there is no ICI.

Also ISI is not an issue here as one symbol duration is 2.5 us while signal round trip time, given by $\frac{2R}{c}$, where r is equal to 25 meters, is 0.168 us. No cyclic prefix is used as the use of cyclic prefix will result in lowering of signal power.

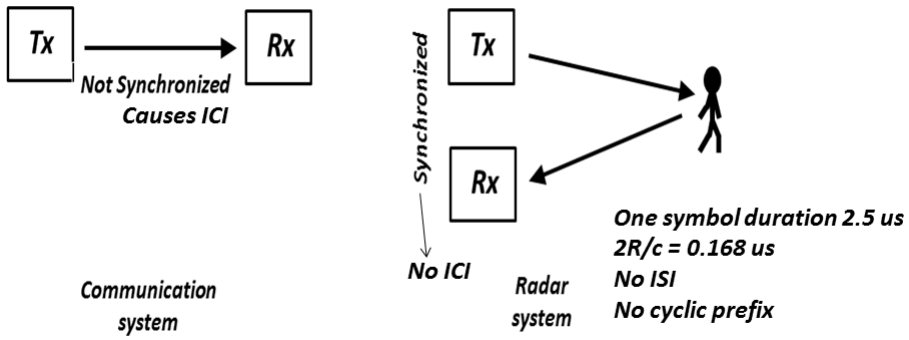

Figure 3-15: Relevance of using OFDM as radar waveform

3.4.1 Distance Measurement on the Basis of Modulation Symbols

With *m = 0*, in eq. (3.5), gives a simplified OFDM single symbol, given by eq. (3.8)

$$x(k)=\sum_{n=0}^{N-1} D_{Tx}(n)e^{\left(\frac{i2\pi nk}{N}\right)}, \text{Where } 0 \le k \le N-1 \quad (3.8)$$

In the presence of the target at a distance of *R* meters from the radar setup, the received OFDM symbol is expressed by eq. (3.9)

$$y(k)=\sum_{n=0}^{N-1} a(n)D_{Tx}(n)e^{\frac{i2\pi n}{T}(-\frac{2R}{c})}e^{(\frac{i2\pi nk}{N})} \quad (3.9)$$

Where, *a(n)* is the amplitude attenuation. The factor of 2 comes into picture as the signal has to travel two times, from radar to the target and back from target to the radar. The signal received sees only attenuation and a phase rotation by a factor of $\frac{2\pi n}{T}(-\frac{2R}{c})$ and increases linearly with each subcarrier. Eq. (3.9) can also be written as in eq. (3.10)

$$y(k)=\sum_{n=0}^{N-1} D_{Rx}(n)e^{(\frac{i2\pi nk}{N})}, \quad where\ 0 \le k \le N-1 \quad (3.10)$$

Comparing this equation with the transmitted equation, eq. (3.9), gives eq. (3.11)

$$D_{Rx}(n) = a(n)D_{Tx}(n)e^{\frac{i2\pi n}{T}(-\frac{2R}{c})} \quad (3.11)$$

In addition to the phase term, the received symbol also contains transmitted modulation symbols which can be easily eliminated by doing element wise complex division [37] as shown in eq. (3.12)

$$I_{div}(n) = \frac{D_{Rx}(n)}{D_{Tx}(n)} = a(n)e^{\frac{i2\pi n}{T}(-\frac{2R}{c})} \quad (3.12)$$

The received symbol is no longer influenced by transmitted modulation symbols. The range information is then computed by taking the IFFT of $I_{div}(n)$ as computed in eq. (3.13)

$$\begin{aligned} Range(k) &= IDFT(I_{div}(n)) \\ &= \frac{1}{N}\sum_{n=0}^{N-1}(I_{div}(n))e^{\left(\frac{i2\pi nk}{N}\right)} \\ &= \frac{1}{N}\sum_{n=0}^{N-1} a(n)e^{\frac{i2\pi n}{T}(-\frac{2R}{c})}\, e^{\left(\frac{i2\pi nk}{N}\right)} \\ &\text{Where, } k=0,1.....N-1 \end{aligned} \quad (3.13)$$

The peak will be given when, $k = \frac{N}{T}(\frac{2R}{C})$ Value of *R* at *k=1* gives the range resolution (in meters) where range resolution is defined as the minimum distance between two targets which the radar system can detect and is given by eq. (3.14)

$$\Delta R = \frac{cT}{2N} = \frac{c}{2BW} \quad (3.14)$$

3.4.2 Speed measurement based on modulation symbols

In the presence of the target moving with a speed of *v m/s* at a distance of *R* meters from the radar setup, the received OFDM symbol is expressed in eq. (3.14) by,

$$y(k)=\sum_{m=0}^{M-1}\sum_{n=0}^{N-1} a(mN+n)D_{Tx}(mN+n)e^{\frac{i2\pi n}{T}(-\frac{2R}{c})}e^{(i2\pi m f_d T)}e^{(\frac{i2\pi nk}{N})} \quad (3.15)$$

The signal received sees only attenuation and a shift of the signal spectrum phase by a factor of $e^{\frac{i2\pi n}{T}(-\frac{2R}{c})}e^{(i2\pi m f_d T)}$

This phase shift destroys the orthogonality between the subcarriers. However, if the subcarrier spacing is kept high, this destruction in orthogonality can be minimized. As per the rule of thumb, $\Delta f \geq 10 f_d$, for the carriers to remain orthogonal. Eq. (3.15) can also be written as shown in eq. (3.16)

$$y(k)=\sum_{m=0}^{M-1}\sum_{n=0}^{N-1} D_{Rx}(mN+n)e^{(\frac{i2\pi nk}{N})} \quad (3.16)$$

Comparing this equation with the transmitted equation, eq. (3.15), gives eq. (3.17)

$$D_{Rx}(mN+n) = a(mN+n)D_{Tx}(mN+n)e^{\frac{i2\pi n}{T}(-\frac{2R}{c})}e^{(i2\pi m f_d T)} \quad (3.17)$$

Now considering single sub carrier, the phase difference is given by $e^{(i2\pi m f_d T)}$, then the resultant received modulation symbols are finally only a dependence of the transmitted modulation symbols [41], the OFDM symbol index *m*, the relative velocity v_{rel} and is given eq. (3.18)

$$D_{Rx}(m) = a(m)D_{Tx}(m)e^{i\varphi_r}e^{(i2\pi m f_d T)} \quad (3.18)$$

A determination of the relative speed of the received modulation symbols is thus only the influence of modulation symbols in the way. This can be evaluated by a simple element-wise complex division of the received and transmitted modulation symbols as shown in eq. (3.19)

$$I_{div}(m) = \frac{D_{Rx}(m)}{D_{Tx}(m)} = a(m)e^{i\varphi_r}e^{(i2\pi m f_d T)} \quad (3.19)$$

And is no longer influenced by transmitted modulation symbols. The velocity information is then computed by taking the DFT of $I_{div}(m)$ as computed in eq. (3.20)

$$Velocity(l)=DFT(I_{div}(m)) \quad (3.20)$$

$$=\sum_{m=0}^{m-1}(I_{div}(m))e^{(-\frac{i2\pi ml}{M})}$$

$$=e^{i\varphi_r}\sum_{m=0}^{m-1} a(m)e^{(i2\pi m f_d T)}e^{(-\frac{i2\pi ml}{M})}$$

Where, l=0,1 .....M-1

The peak will be given when,

$$l=\frac{2v f_c MT}{c} \quad (3.21)$$

In calculating the maximum measurable speed, it must be noted that, in contrast to the measurement, the removal of both positive and negative relative speeds may occur.

Assuming that positive and negative relative speeds occurs, then the largest clearly measurable velocity *v* is given at *l=N/2*

Substituting $l = N/2$ in eq. (3.21) one obtains the minimum detectable velocity.

$$\Delta v = \frac{c}{4 f_c M T} \tag{3.22}$$

3.4.3 Joint determination of distance and speed

Preceding sections shows the determination of range as well as Doppler. But the method described in section 3.4.1 and 3.4.2 fails if two targets are present i.e. it fails in providing information as to which range corresponds to which velocity and vice versa. To address this problem, the two methods are combined to provide two dimensional radar image [40] containing information about both distance as well as speed. Defining such a problem takes matrix representation of transmitted as well as received modulated symbols.

$$D_{Tx}(mN+n) = \begin{pmatrix} d_0 & d_n & d_{2n} & ..... & d_{(m-1)n} \\ d_1 & d_{n+1} & d_{2n+1} & ..... & d_{(m-1)n+1} \\ . & . & . & ..... & . \\ . & . & . & ..... & . \\ d_{n-1} & d_{2n-1} & d_{3n-1} & ..... & d_{mn-1} \end{pmatrix}$$

The columns in the above matrix correspond to one symbol while rows correspond to the data on one subcarrier.

In the presence of the target moving with a speed of *v m/s* at a distance of *R* meters from the radar setup, the received OFDM symbol is expressed in eq. (3.23) by,

$$\mathrm{y}(k) = \sum_{m=0}^{M-1} \sum_{n=0}^{N-1} D_{Rx}(mN+n) e^{\left(\frac{i2\pi nk}{N}\right)} \tag{3.23}$$

Where,

$$D_{Rx}(mN+n) = a(mN+n) D_{Tx}(mN+n).(k_r \otimes k_d)_{m,n}$$

In eq. (3.23), $\otimes$ is the dyalic product and . is the element wise multiplication of matrices.

Here, k_r is a vector that represents the phase delays due to the distance between the target and the radar system, given in eq. (3.24) by

$$k_r = (0 \quad e^{\left(-j2\pi\frac{2R}{CT}\right)} \quad \ldots\ldots \quad e^{\left(-j2\pi(N-1)\frac{2R}{CT}\right)})^T \tag{3.24}$$

And k_d is a vector that represents the Doppler shift, given in eq. (3.25) by

$$k_d = (0 \quad e^{\left(j2\pi T\frac{2cf_c}{c}\right)} \quad \ldots\ldots \quad e^{\left(j2\pi(N-1)T\frac{2vf_c}{c}\right)}) \tag{3.25}$$

Now, to see the influence of range and Doppler alone on the received signal, in eq. (3.23), transmitted modulating symbols needs to be removed. This is done by element wise division, as done previously in section 3.4.1 and 3.4.2, as shown in eq. (3.26)

$$I_{div}(mN+n) = \frac{D_{Rx}(mN+n)}{D_{Tx}(mN+n)} = a(mN+n)\,(k_r \otimes k_d)_{mN+n} \tag{3.26}$$

This leads to a matrix whose column represents range information while rows represent the Doppler information. Therefore, to get the range and Doppler information, IFFT (for range) and FFT (for Doppler) is to be taken on their respective rows and columns as shown in eq. 3.27. Figure 3-16 shows the schematic of OFDM radar system.

$$I(k,l) = DFT(l)[IDFT(k)[I_{div}(m,n)]] \tag{3.27}$$

Where, k=0,1.....N-1

Where, l=0,1.....M-1

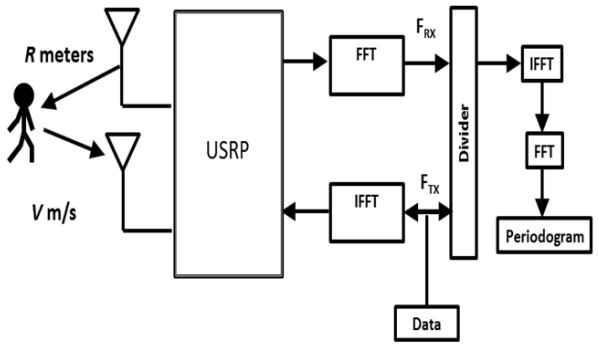

Figure 3-16: Block Diagram of OFDM Radar

Figure 3-17 below shows the graphical representation of above algorithm taken into account transmitted and received modulation symbols. The received modulation symbol, $D_{Rx}(mN+n)$ is divided by transmitted modulation symbol to give $I_{div}(mN+n)$. Now, FFT taken along the time axis to give Doppler information and IFFT is taken along the frequency axis thus giving range information. Since, both FFT and IFFT are independent here, these two steps are interchangeable thus giving range-Doppler radar image.

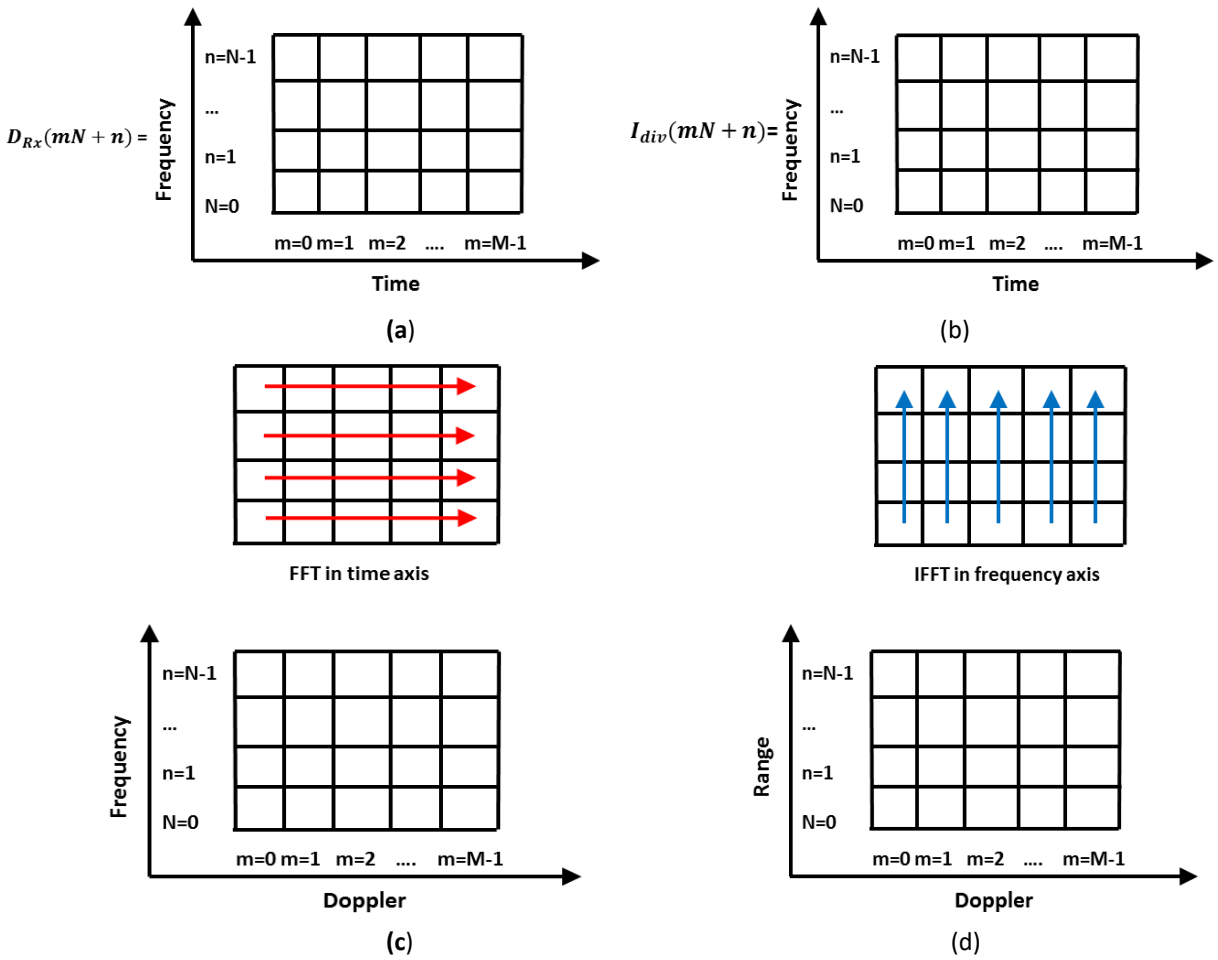

Figure 3-17: OFDM range Doppler Imaging Algorithm

This results in single peak over range bin and single peak over Doppler bin, thus resulting in an image giving information about range and its corresponding velocity. One thing to be kept in mind is that, the velocity of the target should not be high enough that it migrates from its range bin over the integration period. Similarly, a high enough velocity will lead to spreading in Doppler bin.

3.4.4 Micro-Doppler signature extraction using OFDM

The above algorithm provides range Doppler information but does not provide micro-Doppler information. To extract the micro-Doppler information, different OFDM frames are combined in time and then micro-Doppler extraction is carried out. This way, OFDM radar can provide information regarding human movement. Figure 3-18 shows the algorithm used for micro-Doppler extractions using OFDM. After the complex modulation done at the receiver, IFFT is taken along the frequency axis as the system bandwidth (here 400 KHz) is much smaller than the frequency of operation. Hence is assumed that the Doppler affects all the subcarriers by

the same amount. After that, different OFDM frames are combined to increase the total observation time. The Doppler profile can then be determined by taking the STFT along the time axis. Here, bandwidth taken into account is 400 KHz which gives a range resolution of 375 meters (given by $\frac{c}{2BW}$) and the system is tested for 25 meters only, hence, the target will be present in 1 range bin for all the below mentioned cases.

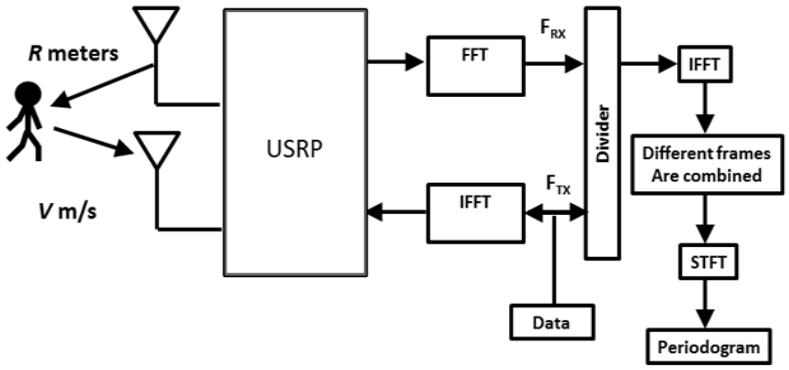

Figure 3-18: Algorithm for micro-Doppler extractions using OFDM

3.4.5 OFDM System Parameterization

The Ethernet port available in the system used is 1 Gb Ethernet port and hence maximum possible data rate (Data rate = Sampling rate*16 as each sample takes a width of 16) or theoretical bandwidth as shown in Figure 3-19 that can be achieved is 25 MSps or 25 MHz [29]. Also in our setup both transmitter and receiver were controlled by 1 system hence the maximum achievable bandwidth is again reduced. For multi-device session, the streaming should be half of single-device but actual performance achieved is much less. This is one of the reported issues in NI and no workaround has been found for this [42].

During implementation, the system set up was not able to support a sampling rate higher than 3 MHz Since sampling rate defines the theoretical bandwidth of the system in USRP, and 3 MHz sampling rate could not have provided required range resolution, hence the system is implemented with bandwidth equals 400 KHz

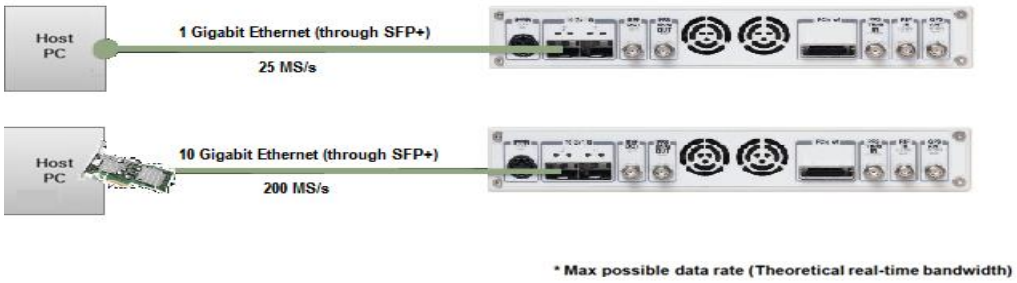

Figure 3-19: USRP RIO interfacing and maximum achievable bandwidth

Figure 3-20 shows the Labview front panel for OFDM transmitter used for implementing radar while OFDM receiver is shown in Figure 3-21

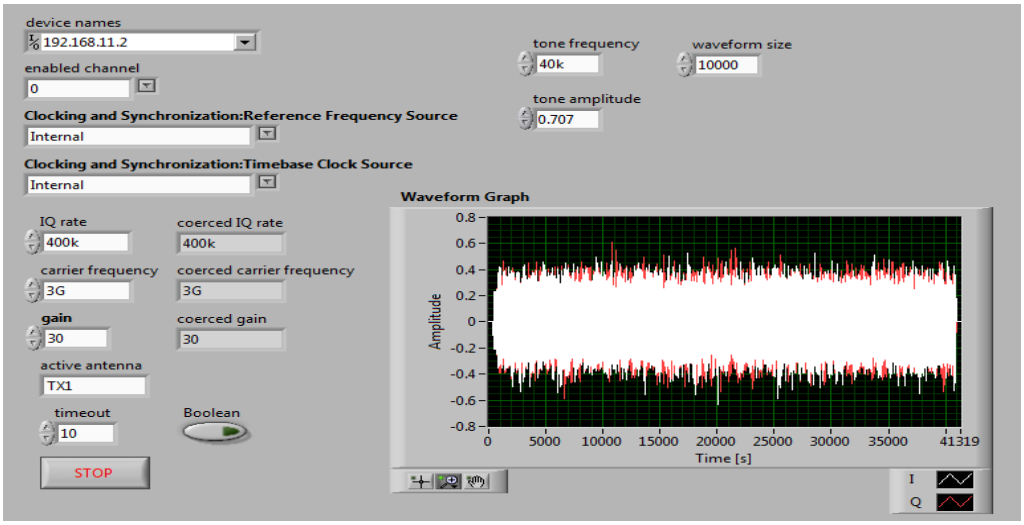

Figure 3-20: OFDM transmitter front panel for radar implementation

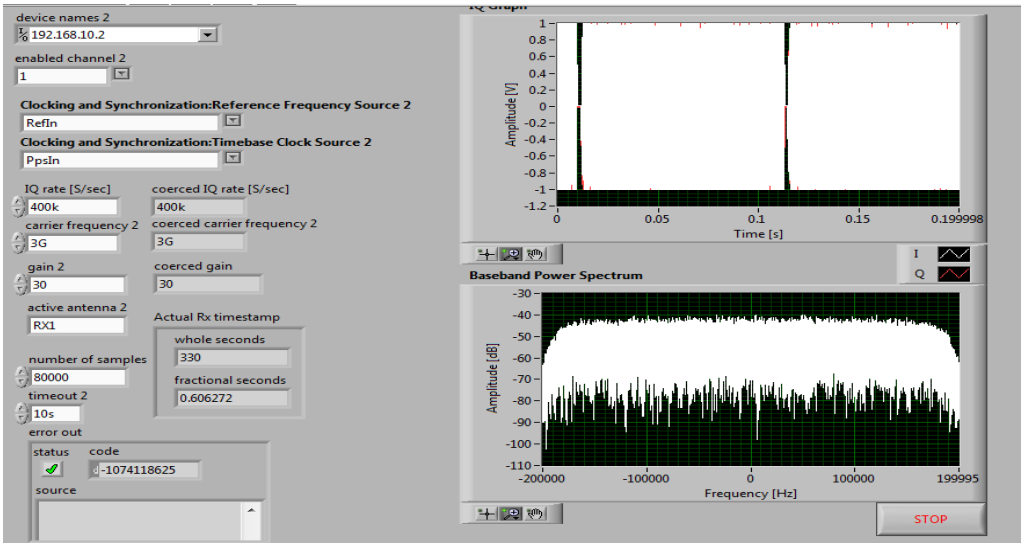

Figure 3-21: OFDM receiver front panel for radar implementation

In this thesis, work has been carried out at I/Q sampling frequency of 400 KS/s. By the Nyquist sampling theorem, if the signal is only being recorded by its In-phase component then the sampling rate needs to be twice the bandwidth of the signal. If both the In-phase and Quadrature are being sampled, then it needs to sample at the same rate as the bandwidth of the signal. Therefore, with a sampling rate of 400 KS/s, bandwidth become equals to 400 KHz.

For implementation of OFDM radar, carrier frequency (f_c) of 3 GHz is chosen with a sampling rate of 400 KS/s and subcarrier spacing (Δf) equals to 6.250 KHz. Elementary OFDM symbol duration, T, given by 1/ Δf, here equals to 0.16 ms. No cyclic prefix has been used. Maximum Doppler frequency that can be observed is given by $\pm 1/2T$, here equals to 3.125 KHz. This corresponds to a velocity range from -85.22 m/s to +85.22 m/s. Doppler resolution depends on the observation period, and is given by fd = 1/(MT) which is equal to 10 Hz giving a velocity resolution of 0.27 m/s. All the system parameters used are summarized in table 3.1.

Table 3.1: OFDM System Parameters

Symbol	Parameter	Value
fc	Carrier frequency	3 GHz
N	Number of subcarriers	64
Δf	Subcarrier spacing	6.250 KHz
T	Elementary OFDM symbol Duration	0.16 ms
B	Bandwidth	400 KHz
Δr	Range resolution	375 m
R_{max}	Maximum unambiguous range	24000 m
V_{max}	Maximum unambiguous Velocity	85.22 m/s
M	Number of evaluated symbols	625
Δv	Velocity resolution	0.27 m/s
Δf	Frequency resolution	9.84 Hz
F_{dmax}	Maximum Doppler frequency	3.125 KHz

Chapter 4

4. Experimental Setup and Results

Experimental setup is designed to implement all the steps in Labview, a visual programming language from National Instruments. For implementation of radar, two USRP 2953R from NI are used - one working as transmitter and other as receiver. The USRPs were synchronized by disabling the clock of the receiver USRP and instead the clock of transmitter USRP was fed into the receiver USRP. A signal of 40 KHz was transmitted over a carrier frequency of 3 GHz and was analyzed at the receiver. Antennas used for the transmission and reception are double-ridged horn antennas as these are wideband antennas having frequency range from 0.8 GHz to 18 GHz. Both the USRPs are connected to the host computer using a 1 GB Ethernet cable. Experiments have been done considering two cases: single human and two humans in free space and in through-wall conditions. Figure 4-1 shows the floor geometry where experiments have been performed. As shown in Figure 4-1 (a), human was made to walk in a corridor while, for through-wall experiments, as shown in Figure 4-1 (b), The human walked behind a brick wall of 12 inches. Human was made to walk behind the wall to capture both the motions - approaching towards the radar system and moving away from the radar system

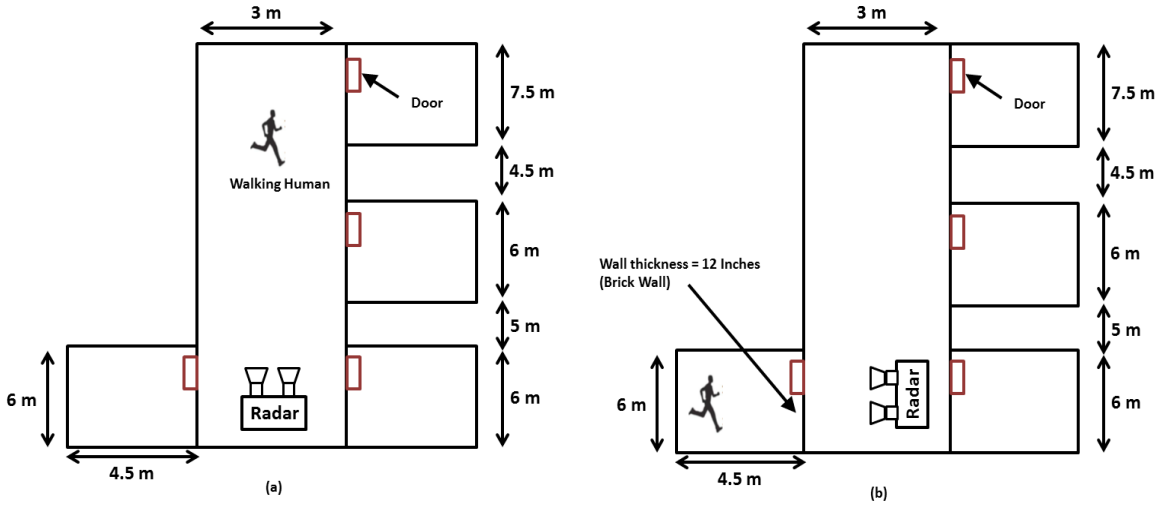

Figure 4-1: Floor geometry (a) For free space experiments (b) For through wall experiments

The human velocity is approximately 2m/s. These results in a Doppler shift of about 60 Hz of the main body and around 200 Hz due to the movement of hands, legs etc. Figure

4-2 shows the block diagram of the experimental setup used and the actual setup used is shown in Figure 4-3.

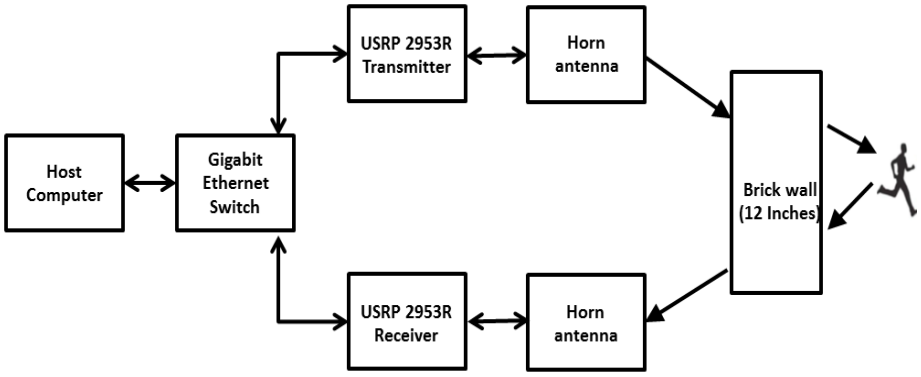

Figure 4-2: Block diagram of the experimental setup

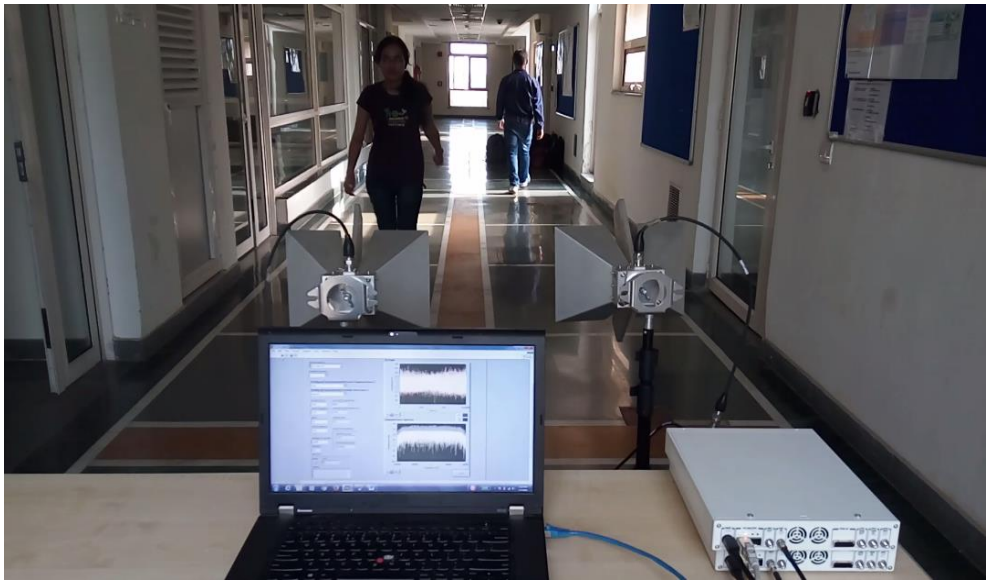

Figure 4-3: Hardware experimental setup

Figure 4-4 shows the simulated micro-Doppler signatures of a human walking motion. Human micro-Doppler as shown in the simulations are based on thalmann model. This model considers 17 point scatters and uses a primitive based modeling where different human body parts are modeled by ellipsoids, spheres, and cylinders. The total scattering from the human is then obtained by adding the returns from all the body parts. Human movement data is then obtained from biomedical field to obtain the trajectory to these points. The mathematical model pertaining to the same is defined in [43]. Figure 4-5 shows the human simulation model, modeled by ellipsoids, spheres and cylinders. The human trajectory is defined by the center of mass of various primitives used.

Here in Figure 4-4 only forward human motion has been considered so the major Doppler shift is seen in the positive direction. Motion of hands, legs and torso has been shown. Also, as the target is moving towards the radar, the received signal power increases. Simulations are carried out at carrier frequency of 3 GHz having a sampling frequency of 1000. The human is assumed to be walking at a speed of 1.12 m/s towards the radar. Data is collected over a time period of 7.5 seconds. The time varying radar cross section (RCS) of the moving human is then calculated by the complex sum of the RCS of the individual body parts modeled as ellipsoids, spheres etc. After obtaining the radar return signals, using the radar equation, STFT is taken over the data with a STFT time window being equal to 0.11 seconds. When seen in a spectrogram, the motion of different body parts is seen to be resolved as shown in Figure 4-4. The strongest returns are from the torso given the fact that RCS of the human torso is greater as compared to other body parts. The highest Doppler shift is caused by the movement of the feet and the head, which is mostly still, does not give rise to significant Doppler. The left and right leg-swing completes one gait cycle. The front and back swings of the human arms and the legs gives rise to both the positive and the negative Doppler with respect to the torso. This is also seen that a human body motion has a slightly saw tooth shape as the body speeds up and slows down every gait cycle.

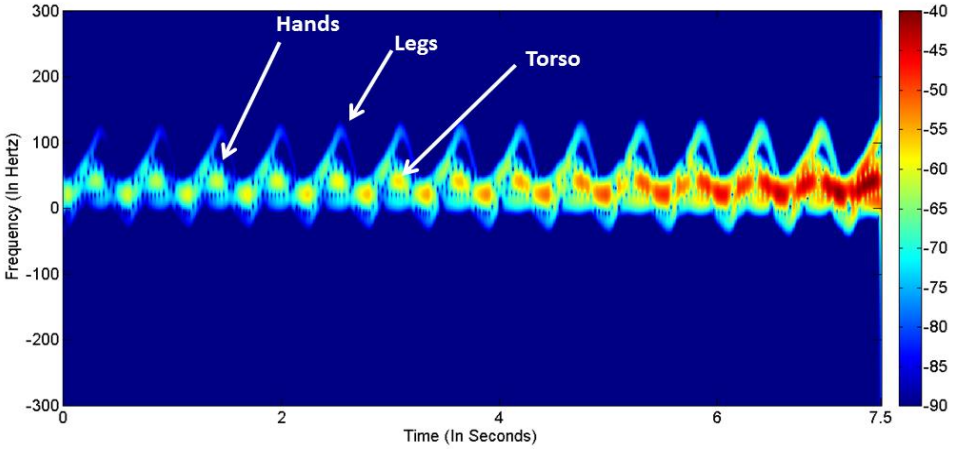

Figure 4-4: Micro-Doppler signature of a walking human

Figure 4-6 shows the human micro-Doppler signatures using CW radar in free space in presence of one human. Here both motions are seen, target approaching the radar as well as going away from the radar. For the first 3.7 seconds, the human is coming towards the radar thereafter human is moving away from the radar. Movements of hands, legs and torso are seen clearly. The difference between the simulation and the experimental results

is because in simulation a 17 point model is considered but in experimental data, whole of the human body is reflecting back the signals. Also, the propagation environment between the human and the radar is quiet complex and introduces significant distortions to the radar signals due to multipath. Also, simulations are carried out considering a constant speed of 1.2 m/s while during experiments, human do not walk at a constant speed for every gait cycle. Human first accelerates, then while turning is almost stationary and then again accelerates as starts moving and decelerates as the human tends to stop. Hence, it is seen that the Doppler shift is different but the pattern of the spectrogram for every gait cycle is same.

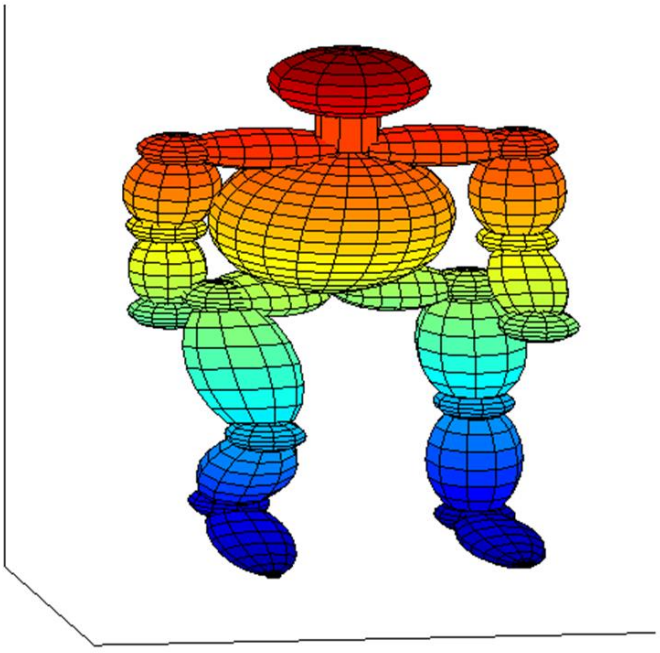

Figure 4-5: Human simulation model

Figure 4-7 shows the human micro-Doppler signatures using CW radar in free space in presence of two human. Both the humans were made to walk in opposite direction i.e. one approaching the radar and the other moving away from the radar. Hence, if one human is giving rise to positive Doppler then the other human is giving rise to negative Doppler and both humans can be distinguished showing movements of different body parts. Also it is seen that the human gait have a similar type of patter and their frequency ranges from 0 Hz to 200 Hz at a carrier frequency of 3 GHz. However, if both the humans are moving in the same direction than the return signals of both human will overlap and hence detection will not be done properly.

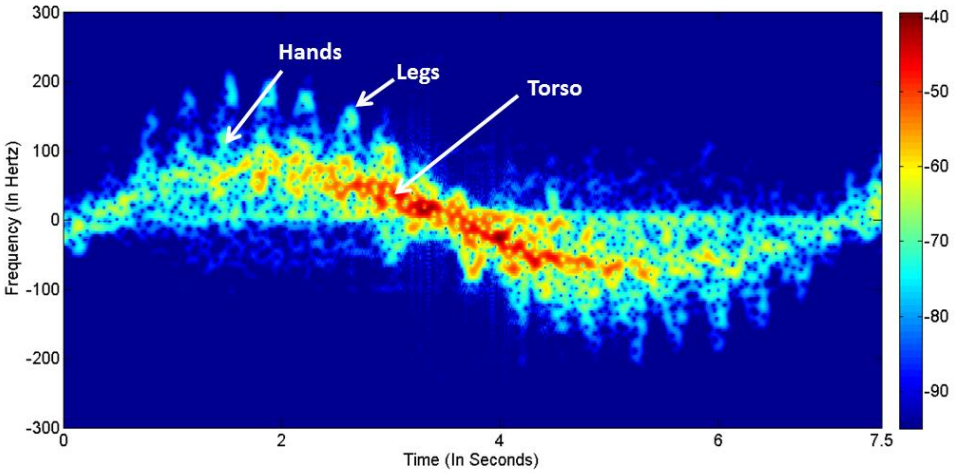

Figure 4-6: Micro-Doppler signatures of single human in free space using CW radar

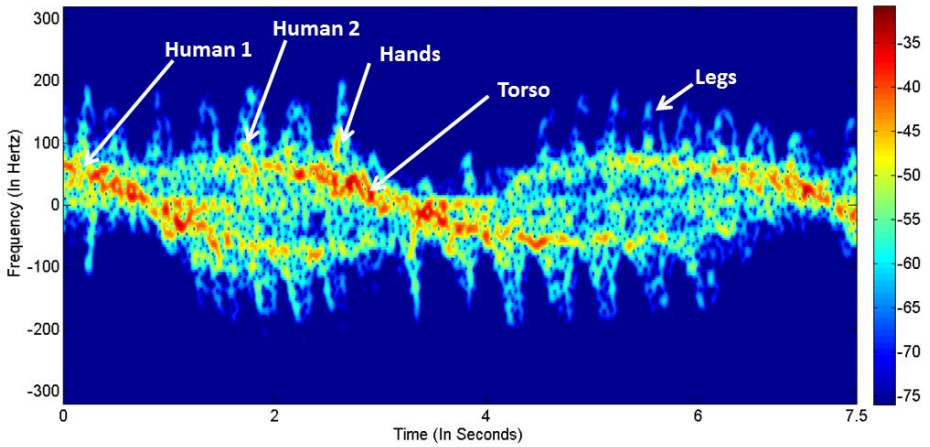

Figure 4-7: Micro-Doppler signatures of two human in free space using CW radar

Figure 4-8 and Figure 4-9 shows the results of human micro-Doppler using CW radar for above mentioned cases in through-wall scenario. In order to compensate for the wall attenuation, an additional 30 dB of amplifier gain was provided to the transmitted signal. Figure 4-8 shows the presence of 1 human in across the wall while presence of two human was shown in Figure 4-9. The Doppler returns are not clean as compared to that of the Figure 4-6 and Figure 4-7 but that does not have any significant effect in detection of human Doppler as compared to human in free space. As stated earlier in section 1.1, walls are dispersive medium providing multipath and scattering to the signal, this is seen clearly from the above figures. The micro-Doppler signatures in case of through-wall are scattered as compared to that of free space and additional signal processing is required to nullify the wall effects but this is quite challenging as the wall taken under consideration do not have uniform properties and we do not have the wall properties available to us.

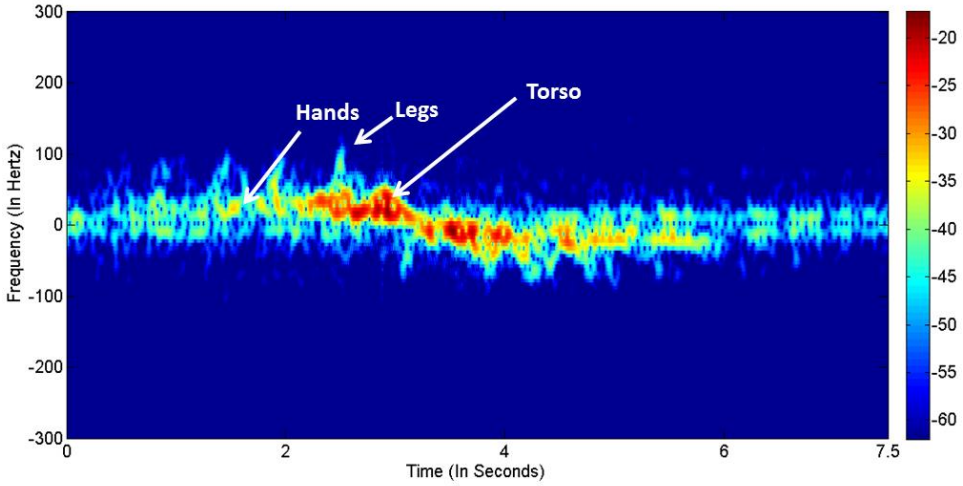

Figure 4-8: Micro-Doppler signatures of single human behind wall using CW radar

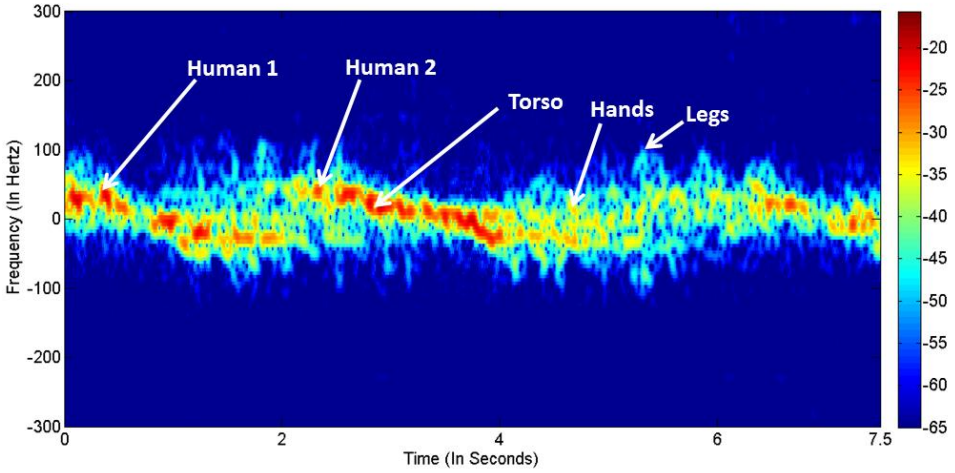

Figure 4-9: Micro-Doppler signatures of two human behind wall using CW radar

Figure 4-10 and Figure 4-11 shows the range-Doppler profile using OFDM radar in presence of single human and two human in free space. Figure 4-10 shows the presence of 1 human in free space while presence of two human was shown in Figure 4-11.

Through wall range-Doppler profile is shown in Figure 4-12 and Figure 4-13, with single human present in Figure 4-12 and the presence of two human is shown in Figure 4-13.

The range-Doppler processing only gives information about the location of human and the average Doppler but does not give any information about the micro-Doppler of the human. Also, In case of OFDM radar, the transmitted power distributes throughout the bandwidth hence the received signal strength decreases as compared to that of the CW radar. The strong reflection shown in Figure 4-10 - Figure 4-13 is due to the direct signal off the target and the wall. Here, both the targets are present in the same range bin

as our system bandwidth was less and hence are seen in the first bin only. In all the above mentioned figures, m-Dr are visible side to the bulk body but since there is no timing information in these plots hence the activity or the profile of human is hard to deduce.

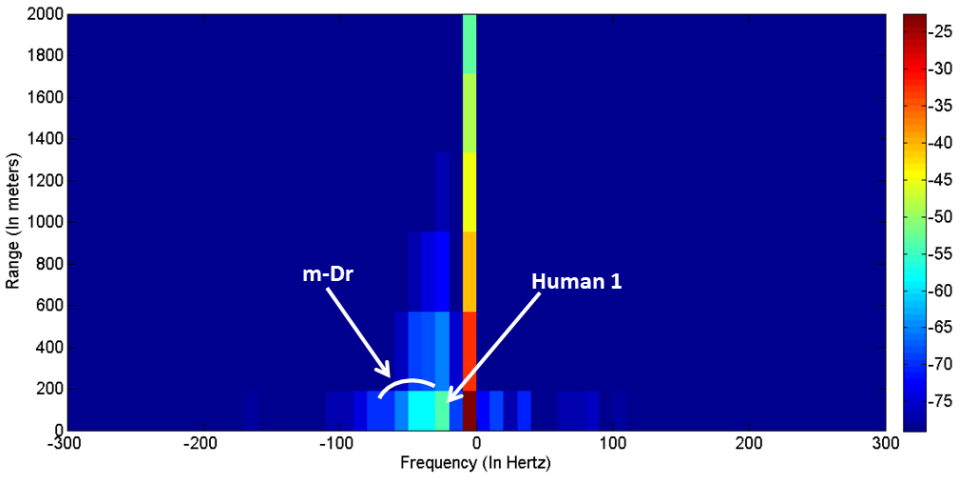

Figure 4-10: Range-Doppler profile of single human using OFDM in free space

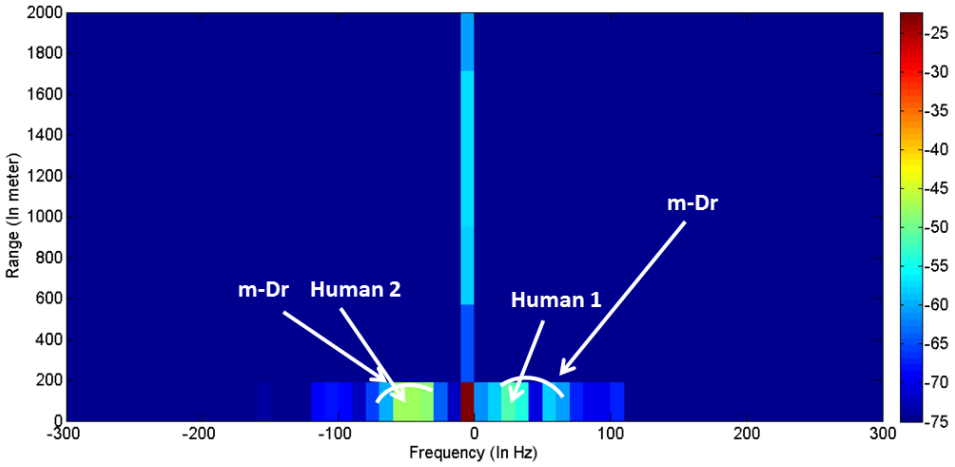

Figure 4-11: Range-Doppler profile of two human using OFDM in free space

Here, in Figure 4-10 - Figure 4-13, humans behind the wall can be differentiated from that of the free space environment by comparing the magnitude. Here, since in both the cases, transmitted power is kept same, and as can be seen in Figure 4-10 - Figure 4-13 received power is -25 dBm while in case of through wall it is -50 dBm. As the wall provides sufficient attenuation, the received power in case of through wall decreases but again this does not have any significant effect on detection of human range and Doppler.

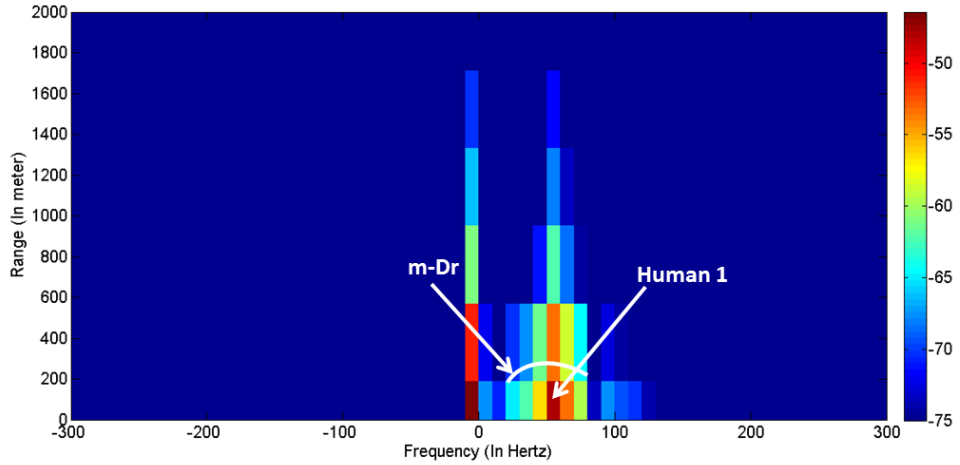

Figure 4-12: Range-Doppler profile of single human using OFDM in through wall

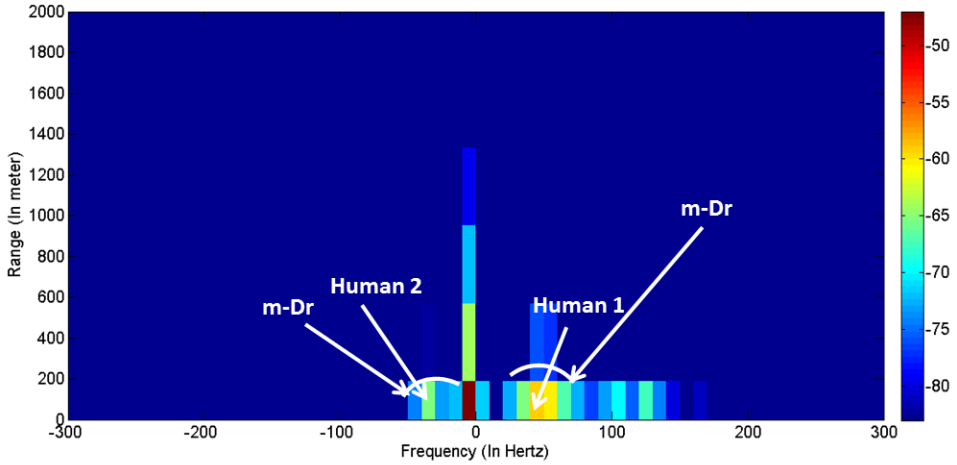

Figure 4-13: Range-Doppler profile of two human using OFDM in through wall

Figure 4-14 - Figure 4-17 shows the micro-Doppler signatures of human due to OFDM radar. Figure 4-14 shows the presence of single human in free space using OFDM radar while Figure 4-15 shows the presence of two human moving in opposite directions. In Figure 4-14, human first walks towards the radar and then walks away from the radar while in Figure 4-15, two humans were walking opposite to each other. While detecting in micro-Doppler, since number of frames were integrated to increase the sweep time, this leads in getting the micro-Doppler signatures of the human.

Similarly, Figure 4-16 shows the presence of single human behind the wall using OFDM radar while Figure 4-17 shows the presence of two human moving in opposite direction.

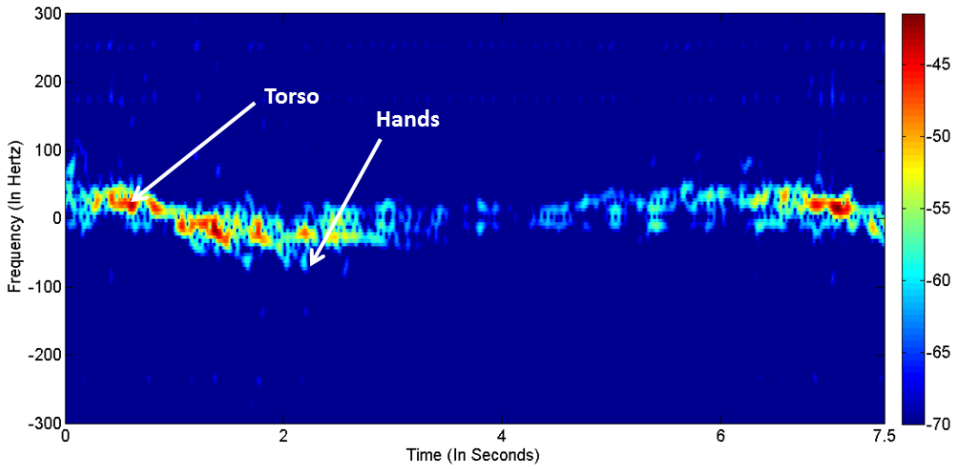

Figure 4-14: Micro-Doppler signatures of single human in free space using OFDM radar

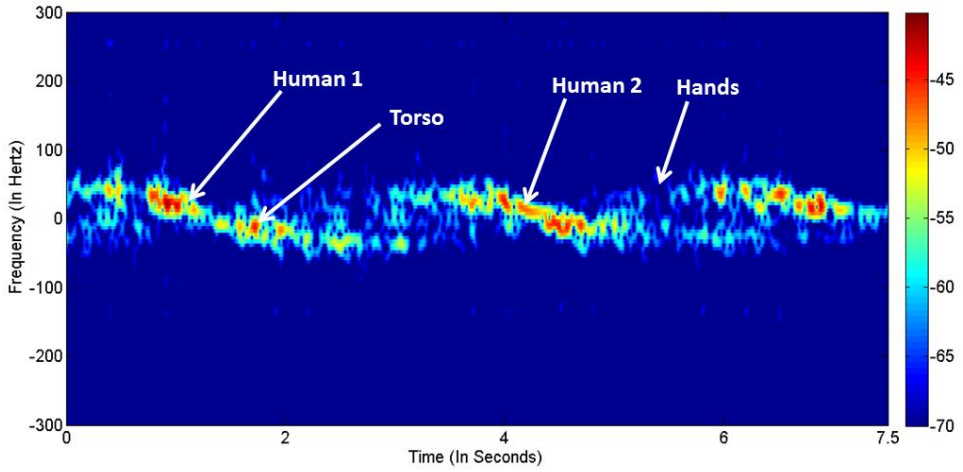

Figure 4-15: Micro-Doppler signatures of two human in free space using OFDM radar

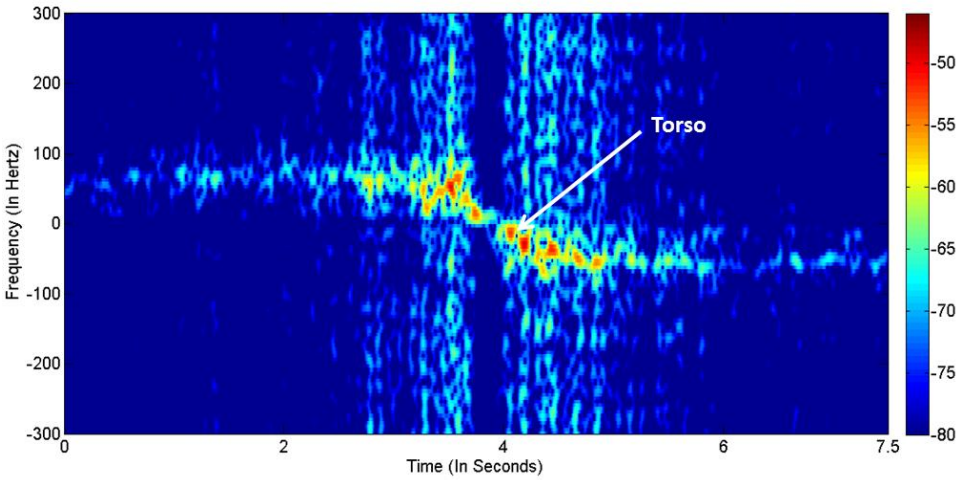

Figure 4-16: Micro-Doppler signatures of single human behind wall using OFDM radar

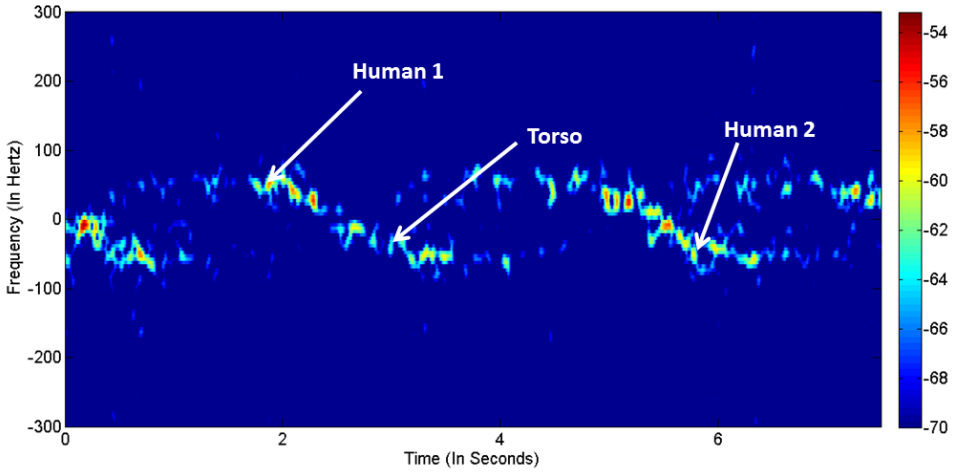

Figure 4-17: Micro-Doppler signatures of two human behind wall using OFDM radar

In all the above shown Micro-Doppler signatures of human using OFDM i.e. from Figure 4-14 - Figure 4-17, it is seen that for through wall scenario, only torso movement is shown, the detection of hands, legs and other body parts are difficult to see. This is accounted due to less received power in through wall case due to the attenuation provided by the wall and the fact that the RCS of hands and legs are lesser as compared to that of the torso. Also the signatures are discontinuous as we have guard band present between different OFDM frames and detection is done using only the complex modulated symbols. Here also, in Figure 4-17 and Figure 4-17, if one human is giving rise to positive Doppler then the other human is giving rise to negative Doppler and both humans can be distinguished showing movements of different body parts. However, if both the humans are moving in the same direction than the return signals of both human will overlap and hence detection will not be done properly.

OFDM radar signals using different signals processing, is able to give information about both the range-Doppler as well as micro-Doppler of the moving human in free space as well as behind the wall while CW radar gives information of micro-Doppler signatures of human.

Chapter 6

5. Conclusion

CW and OFDM radar have been implemented on a USRP platform. The CW radar provides only the micro-Doppler information while the OFDM radar is able to provide both range and Doppler information. Micro-Doppler extraction is also carried out using OFDM radar by stacking different OFDM frames. Both type of radar are tested in presence of single human and multiple humans. Both the radars have been implemented in free space and through-wall conditions.

CW radar requires less power to operate as compared to OFDM radar but CW radar cannot provide range information. CW radar is easy to implement and requires less computation effort with no discontinuity, but does not provide range information. Hence, CW radar is a better option if only micro-Doppler signatures are required but if one wants to know the distance of the target than OFDM radar is a better option.

Also, USRPs are an appropriate platform for the implementation of radar systems providing flexibility in changing the carrier frequency, waveform and post processing. The only limitation is of USRP being not calibrated and requires extra efforts in calibration. As power plays an important role in radars, extra power amplifiers can be used to enhance micro-Doppler signatures.

Radar micro-Doppler signatures can be used in identifying the activity of human like walking, running, jogging and can also detect the distance of target from the radar setup. Though wall has result in scattering of the signal but human activity is still detectable and hence we can say that radar signatures can be used in military, search and rescue operations and is not affected by the presence of obstacle in between.

Future work

As USRP RIO has two independent transmitter and receiver chains, hence the above work can be extended to see the direction of arrival, azimuth and elevation of the target so as to get the exact position of the human. Also wall provides variable attenuation to the signal hence, Waveform designing can be done to mitigate the effect of the wall. Also it is seen that the presence of interfering signals like WIFI affect the radar performance. Waveform designing can also be done to mitigate the effect of this interference and hence increasing the signal to noise ratio.

References

1. D. M. Gavrila, "The visual analysis of human movement: A survey" *Computer vision and image understanding*, Vol. 73, No. 1, pp. 82–98, 1999.
2. D. Zhang, F. Xia, Z. Yang, L. Yao and W. Zhao, "Localization technologies for indoor human tracking" *5th International Conference on Future Information Technology*, IEEE, 2010.
3. C. Wolff, "Physical fundamentals of the radar principal" retrieved online at: http://www.radartutorial.eu/01.basics/Physical%20fundamentals%20of%20the%20radar%20principle.en.html
4. D. J. Daniels "Ground penetrating radar", *Institution of electronics and communication*, Vol. 1. , 2004.
5. O. Hunaidi and P. Giamou "Ground-penetrating radar for detection of leaks in buried plastic water distribution pipes" *Seventh International Conference on Ground-Penetrating Radar*, Lawrence, Kansas, USA, 1998.
6. V. N. Bringi and V. Chandrasekar, "Polarimetric Doppler weather radar: principles and application" *Cambridge University Press*, 2001.
7. J. Sachs, M. Aftanas, S. Crabbe, M. Drutarovsky, R. Klukas, D. Kocur, T.T. Nguyen, P. Peyerl, J. Rovnakova, and E. Zaikov "Detection and tracking of moving or trapped people hidden by obstacles using ultra-wideband pseudo-noise radar" *Radar Conference*, IEEE, 2008.
8. P. Andreas, and R Price, "From war fighting to crime fighting: transforming the American national security state" *International Studies Review* Vol. 3, No. 3, pp. 31-52, 2001.
9. J. E. Peabody, G. L. Charvat, J. Goodwin, and M. Tobias "Through-wall imaging radar*" Lincoln Laboratory journal*, Vol. 19, No. 1, pp. 62-72, 2012.
10. R. M. Narayanan, M. C. Shastry, P.H. Chen, and M. Levi, "Through-the-wall detection of stationary human targets using Doppler radar" *Progress In Electromagnetics Research* B, Vol. 20, 147-166, 2010.
11. O. Josef, "Method and apparatus for body position monitor and fall detect ion using radar" *U.S. Patent* No. 7,916,066 B1, 29 Mar. 2011
12. H. Burchett, "Advances in through wall radar for search, rescue and security applications*" The Institution of Engineering and Technology Conference on crime and security*, 2006.
13. T. Debatty, "Software defined RADAR a state of the art," *2nd International Workshop on Cognitive Information Processing*, 2010.
14. J. Ralston and C. Hargrave. "Software defined radar: An open source platform for prototype GPR development." *14th International Conference on Ground Penetrating Radar (GPR)*, IEEE, 2012.
15. J. Mendoza, "Development of an Ice-penetrating Software-defined Radar" (Dissertation), retrieved from *The Pennsylvania State University*, 2012.
16. B. Godana, G. Leus and A. Barroso, "Quantifying human indoor activity using a software radio-based radar" *First International Conference on Sensor Device Technologies and Applications (SENSORDEVICES)*, IEEE, 2010.
17. B. Godana, G. Leus and A. Barroso, "Estimating human movement parameters using a software radio-based radar" *International Journal on Advances in Systems and Measurements*, Vol. 4, No. 1-2, 2011
18. S. Costanzo, F. Spadafora, A. Borgia, H. O. Moreno, A. Costanzo and G. Di Massa1, "High resolution software defined radar system for target detection" *Journal of Electrical and Computer Engineering- Special issue on Advances in Radar Technologies*, vol. 206, pp. 997-1005, 2013.
19. H. D. Griffiths and C. J. Baker, "Fundamentals of tomography and radar" *Advances in Sensing with Security Applications*, Springer Netherlands, pp. 171-187, 2006
20. J. F. Walker, D. G. Gonzalez, A. Kelkar and N. Lamarra, "Digital beamforming radar system" *U.S. Patent* No. 6,882,311 B2, 19 Apr. 2005.
21. M. G. Anderson and R. L. Rogers, "Micro-Doppler analysis of multiple frequency continuous wave radar signatures" *Defense and Security Symposium,* International Society for Optics and Photonics, 2007.
22. V. C. Chen, D. Tahmoush and W. J. Miceli, "Radar micro-Doppler signatures: processing and applications", *The institution of engineering and technology*, Vol. 34. 2014.

23. B. Tan, “University College London Tracks WiFi Signals to Passively See Through Walls Using NI Wireless Design Tools”, *NI case study*, retrieved online at: http://sine.ni.com/cs/app/doc/p/id/cs-16238#
24. M. G. Amin and F. Ahmad, "Through-the-wall radar imaging: theory and applications" *Radar Signal Processing Section, E-Reference Signal Processing, Elsevier*, 2013.
25. L3 communications, Cyterra, “RANGE-R Handheld through-wall sensor, When every second counts” retrieved online at: http://www.range-r.com/documents/RANGER.pdf
26. P. K. Verma, A. N. Gaikwad, D. Singh, and M. J. Nigam, "Analysis of clutter reduction techniques for through wall imaging in UWB range" *Progress In Electromagnetics Research B*, Vol. 17, pp. 29-48, 2009.
27. National Instruments, “An Introduction to Software Defined Radio With LabVIEW and NI USRP” April 2015, retrieved online at: http://www.ni.com/white-paper/14518/en/
28. National Instruments, “2 × 2 MIMO With NI USRP” Aug 24, 2015, retrieved online at http://www.ni.com/white-paper/13878/en/
29. National Instruments, “Overview of the NI USRP Rio Software Defined Radio” Dec 14, 2015, retrieved online at http://www.ni.com/white-paper/52119/en/
30. Rohde and Schwartz , “R&S HF907 Double Ridged Horn Antenna” retrieved online at: https://www.rohde-schwarz.com/us/product/hf907-productstartpage_63493-7982.html
31. National Instruments, “NI USRP-2921 block diagram”, retrieved online at: http://zone.ni.com/reference/en-XX/help/373380B-01/usrphelp/2921_block_diagram/, 2012
32. National Instruments, “NI USRP-2922 block diagram”, retrieved online at: http://zone.ni.com/reference/en-XX/help/373380B-01/usrphelp/2922_block_diagram/, 2012.
33. C. Wolff, “Continuous wave radar” retrieved online at: http://www.radartutorial.eu/02.basics/Continuous%20Wave%20Radar.en.html
34. A. J. Jones, "Implementation of a Pulsed Radar System on Open Source Software and Hardware" (Dissertation), *University of Cape Town, Cape Town*, 2013.
35. J. L. Geisheimer, W. S. Marshall, and E. Greneker, "A continuous-wave (CW) radar for gait analysis" *Thirty-Fifth Asilomar Conference on Signals, Systems and Computers, IEEE*, Vol. 1, 2001.
36. S. Nawab, T. Quatieri and J. Lim, "Signal reconstruction from short-time Fourier transform magnitude" *IEEE Transactions on Acoustics, Speech, and Signal Processing*, Vol. 31, No. 4, pp. 986-998, 1983.
37. C. Sturm, T. Zwick, and W. Wiesbeck "An OFDM System Concept for Joint Radar and Communications Operations" *Vehicular Technology Conference,* 2009.
38. G.E.A. Franken, H. Nikookar and P. V. Genderen, “Doppler tolerance of OFDM-coded radar signals” *European Radar Conference*, 2006.
39. Y. L. Sit, C. Sturm, L. Reichardt, W. Wiesbeck and T. Zwick, “Verification of an OFDM-based range and Doppler estimation algorithm with ray-tracing” *IEEE-APS Topical Conference on Antennas and Propagation in Wireless Communications (APWC),* 2011.
40. Y. L. Sit, C. Sturm, L. Reichardt, T. Zwick and W. Wiesbeck, "The OFDM joint radar-communication system: An overview*" Advances in Satellite and Space Communications (SPACOMM),* 2011.
41. Y. L. Sit, C. Sturm, and T. Zwick "Doppler estimation in an ofdm joint radar and communication system" *German Microwave Conference*, IEEE, 2011.
42. National Instruments, “NI-USRP 1.0 and 1.1 known issues” May 17,2012, retrieved online at: http://www.ni.com/product-documentation/13162/en/
43. R. Boulic, N.M. Thalmann and D. Thalmann, “A global human walking model with real-time kinematic” *The Visual Computer*, vol.6, pp.344-358, 1990